ELSEVIER

Materials Science and Engineering A327 (2002) 167–185

MATERIALS SCIENCE & ENGINEERING A

www.elsevier.com/locate/msea

Directional solidification of aluminium–copper alloys

M. Gündüz [a,*], E. Çadırlı [b]

[a] *Department of Physics, Faculty of Arts and Sciences, Erciyes University, 38039 Kayseri, Turkey*
[b] *Department of Physics, Faculty of Arts and Sciences, Niğde University, 51100 Niğde, Turkey*

Received 14 June 2000; received in revised form 31 May 2001

Abstract

Directional solidification experiments have been carried out on different Al–Cu alloys as a function of solidification parameters, temperature gradient G, growth rate V, and composition C_0. The specimens were solidified under steady state conditions with a constant temperature gradient (7.4 K mm^{-1}) at a wide range of growth rates (9–490 μm s^{-1}) and with a constant growth rate of 9.5 μm s^{-1} at a wide range of temperature gradients (1.0–7.4 K mm^{-1}). Microstructural parameters, the primary dendrite arm spacing λ_1, secondary dendrite arm spacing λ_2, dendrite tip radius R, mushy zone depth d were measured and expressed as functions of solidification parameters, G, V and C_0 by using a linear regression analysis. The results were in good agreement with previous experimental work and current theoretical models suggested for dendritic growth.

Keywords: Al–Cu alloys; Directional solidification; Primary dendrite arm spacing; Secondary dendrite arm spacing; Dendrite tip radius; Mushy zone depth

1. Introduction

Dendritic structures are frequently observed during the solidification of alloys. The presence of dendritic structures during solidification, with concomitant microsegregations, is of great interest since these solidification features are commonly found in many engineering materials and furthermore, greatly influence the mechanical behavior [1,2]. Solidification interface morphology has been focused by many metallurgists, physicists and mathematicians for the past four decades, and several directional solidification studies have been carried out to predict growth conditions for development of instability at the solid–liquid interface and to characterize the microstructural features, especially the primary dendrite arm spacing, λ_1 [1–61], secondary dendrite arm spacing λ_2 [41–65], dendrite tip radius R [36–51,62–69], and mushy zone depth d [34,35,70–74] as functions of solidification conditions.

In a directional solidification experiment, the planar interface becomes unstable at the grain boundary, and then the entire interface develops a periodic profile. As the interface velocity increases, a cellular pattern develops which subsequently transforms into a dendritic structure. Microstructural characteristics of the dendritic front (primary dendrite arm spacing, dendrite tip radius, mushy zone depth) reach constant values during steady-state solidification. In contrast, the secondary dendrite arms coarsen in time. However, the first few side branches, initial secondary spacing λ_2, always form with a characteristic spacing [41]. Thus, we may characterize dendritic structures with their four steady state microstructural parameters (λ_1, λ_2, R and d).

In directional solidification experiments, solidification parameters, G and V may be independently controlled so that one may study the dependence of microstructural parameters (λ_1, λ_2, R and d) on either G at constant V or V at constant G for the constant initial solute composition C_o. Most experimental studies [1–26, 28, 34–37, 41–47, 49, 50, 52–67, 70, 71, 75, 76] have shown that the microstructural parameters (λ_1, λ_2, R and d) decrease as solidification parameters (G, V) increase, for the constant C_o. The above observations have led, over the past decades, to the establishment of relationships between the solidification and microstructural parameters. A literature survey shows several

* Corresponding author. Tel.: +90-352-437-5262; fax: +90-352-437-4933.
E-mail address: gunduz@erciyes.edu.tr (M. Gündüz).

0921-5093/02/$ - see front matter
PII: S0921-5093(01)01649-5

theoretical studies [27,29–33,48,51,62,68,69,72–74] and theoretical models [33,38–40] used to examine the influence of solidification parameters (G, V, C_o) on the microstructural parameters (λ_1, λ_2, R, d).

1.1. Primary dendrite arm spacing

Theoretical models have been proposed in the literature to describe λ_1 as a function of V, G and C_o by Hunt [38], Kurz and Fisher [39], Trivedi [40] and Hunt and Lu [33]. Hunt attempted to allow for the interaction of the diffusion fields between neighboring cells using an approach suggested by Bower et al. [77]. The relationship between the solidification parameters (G, V, C_o) and λ_1 for a spherical dendritic front with the growth condition for dendrites is determined by the minimum undercooling [29,30,48,68,69]. The Hunt model gives,

$$\lambda_1 = 2.83[m(k-1)D\Gamma]^{0.25}C_0^{0.25}V^{-0.25}G^{-0.5} \quad (1)$$

where m is liquidus slope, k is partition coefficient, D is diffusion coefficient in liquid and Γ is Gibbs–Thomson coefficient.

Another theoretical model to characterize λ_1 as function of G, V, C_o was developed by Kurz and Fisher [39]. Kurz and Fisher assumed that the shape of the cell or dendrite can be approximated as ellipsoids and using the marginal stability criterion for an isolated dendrite or cell and they simplified their results for the low velocity ($V < V_{cs}/k$) and for the high velocity ($V > V_{cs}/k$) regimes (where V_{cs} is the critical velocity at which the planar interface becomes unstable). For $V > V_{cs}/k$ they obtained.

$$\lambda_1 = 4.3[m(k-1)D\Gamma/k^2]^{0.25}C_0^{0.25}V^{-0.25}G^{-0.5} \quad (2)$$

The other theoretical model to characterize λ_1 as function of G, V, C_o was developed by Trivedi [40]. Trivedi model is a result of the Hunt model modification, and used marginal stability criterion. Trivedi model gives

$$\lambda_1 = 2.83[m(k-1)D\Gamma L]^{0.25}C_0^{0.25}V^{-0.25}G^{-0.5} \quad (3)$$

where L is a constant that depends on the harmonic perturbations. These theoretical models are very similar at high growth rate for λ_1 and the difference among them is a constant only. We compare the theoretical models for high growth rate because our experiments were carried out for high growth rates ($V > V_{cs}$) and the experimental results were compared with the results obtained with the theoretical models.

Recently, Hunt and Lu [33] have investigated the cellular/dendritic array growth by using a numerical model. They presented analytic expressions that fitted the numerical results. According to the Hunt–Lu model, in the absence of convection and the dimensionless primary dendrite arm spacing is given by

$$\lambda' = 0.07798V'^{(a-0.75)}(V'-G')^{0.75}G'^{-0.6028} \quad (4)$$

where, $\lambda = \lambda\Delta T_0/(\Gamma k)$, $G = G\Gamma k/(\Delta T_0)^2$, $V = V\Gamma k/(D\Delta T_0)$, $\Delta T_0 = mC_0(k-1)/k$ and $a = 1.131 - 0.1555 \log G - 0.007589 (\log G')^2$.

1.2. Secondary dendrite arm spacing

Langer and Müller-Krumbhaar [62] have carried out a detailed numerical analysis of the wavelength of instabilities along the sides of a dendrite and have predicted scaling law as $\lambda_2/R = 2$. Using the scaling law $\lambda_2/R = 2$, the variation in λ_2 for small peclet number conditions given by Trivedi and Somboonsuk [41] as

$$\lambda_2 = (8\Gamma D\mathrm{L}/k\mathrm{V}\Delta T_0)^{0.5}. \quad (5)$$

1.3. Dendrite tip radius

As mentioned in the previous section, the Hunt model [38], the Kurz–Fisher model [39] and Trivedi model [40] have been applied to find the relationships between R as a function V and C_o. According to the Hunt model [38],

$$R = [2\Gamma D/m(k-1)]^{0.5}C_0^{-0.5}V^{-0.5} \quad (6)$$

whereas the Kurz–Fisher model [39]

$$R = 2\pi[\Gamma D/m(k-1)]^{0.5}C_0^{-0.5}V^{-0.5} \quad (7)$$

and according to the Trivedi model [40],

$$R = [2k\Gamma D/m(k-1)]^{0.5}C_0^{-0.5}V^{-0.5}. \quad (8)$$

As can be seen from Eq. (6),Eq. (7) and Eq. (8) the theoretical models for R also are very similar and the difference among them is a constant only.

1.4. Mushy zone depth

The mushy zone depth, d is defined as the distance between the tip and the root of a dendrite trunk. Using constitutional supercooling criterion [46,47] for binary alloy systems in the absence of convection d is given by

$$d \approx m(C_E - C_0)/G \quad (9)$$

where C_E is eutectic composition. d assumed to be equal to the distance between the liquidus temperature T_L corresponding to $C_t (C_t \cong C_o)$ and the solidus temperature T_S corresponding to C_L which is equal to C_E when $C_o > C_{SE}$ (see Fig. 1). Using the phase diagram, the temperature difference between the liquidus line and the solidus line is given [79] as,

$$\Delta T_0 = -m\Delta C_0 = T_L - T_S. \quad (10)$$

By using Eq. (9) and Eq. (10) d can be expressed as,

$$d = \frac{\Delta T_o}{G}. \quad (11)$$

Inspection of the available literature indicates that the models proposed by Hunt [38], Kurz and Fisher [39], Trivedi [40] and Hunt and Lu [33] have been successfully utilized to provide insight into the resultant solidification morphologies of different materials grown under a wide variety of conditions, despite the differing assumptions involved.

The purpose of the present work is to experimentally investigate the relationship between solidification parameters (G,V) and the microstructural parameters (λ_1, λ_2, R, d), and to compare the results with the previous experimental results and the existing theoretical model and see the effect of composition on microstructural parameters. Al–Cu system has been chosen for the study because of its most available experimental results and well defined physical properties.

2. Experimental procedure

Different Al–Cu master alloys (Al–(3, 6, 15, 24) wt.% Cu) were prepared by melting weighed quantities of Al and Cu of high purity elements (99.99%) in a graphite crucible inserted into the vacuum melting furnace [80]. After allowing time for melt homogenisation, molten alloy was poured into the prepared 13 graphite crucibles (250 mm in length 4 mm ID and 6.35 mm OD) in a hot filling furnace. Each specimen was positioned in a Bridgman type furnace in a graphite cylinder (300 mm in length 10 mm ID and 40 mm OD). After stabilizing the thermal conditions in the furnace under an argon atmosphere, the specimen was grown by pulling it downwards at various constant rates by means of different speed synchronous motors. Specimens were solidified under steady state conditions with a constant growth velocity (approx. 9.5 μm s^{-1}) and different temperature gradients (1.0–7.4 K mm^{-1}), with a constant temperature gradient (approx. 6.3 K mm^{-1}) and different growth rates 9–490 μm s^{-1} (Table 1). After 100–120 mm steady state growth of the samples, they were quenched by pulling them rapidly into the water reservoir. Also, in order to see the composition effect on structure parameters, directional solidification experiments were repeated for four different Al–Cu alloys which cover the Al rich side of the Al–Cu phase diagrams (Fig. 1).

2.1. Measurement of temperature gradient, G and growth rates, V

The temperature of the Bridgman type furnace was controlled by a Pt/Pt–13%Rh thermocouple placed between the heating element and the alumina tube. The temperature could be controlled to about ±0.1 K during the run. Throughout the experiment, the thermocouples were placed into the capillary alumina tubes (0.8 mm ID, 1.2 mm OD) which were positioned approx. 20 mm apart and parallel to the heat flow direction inside the crucible. Temperature distribution was obtained by measuring the temperature in the sample during the heating and cooling by five chromel/alumel thermocouples (type-K) which were placed in the sample (The experimental details are given in Ref. [81].) Accuracy of the thermocouples was checked by slowly solidifying the Al–Cu samples (which where thermocouples placed parallel to the heat flow and perpendicular to the heat flow direction). The measured T_e difference was less than 0.5 K with differently placed thermocouples. All the thermocouple leads were taken to an ice/water cold junction, then to a WPA analog potentiometer and to a Kipp–Zonen chart recorder

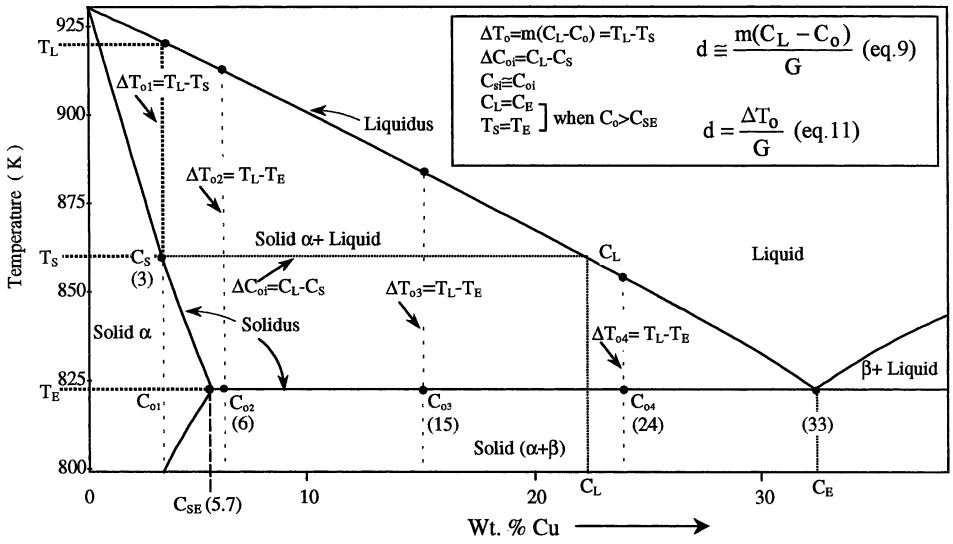

Fig. 1. Al–Cu phase diagram [78] shows definition of C_{oi}, ΔC_{oi} and ΔT_{oi}.

Table 1
Variation of experimental microstructural parameters (λ_1, λ_2, R, d) with solidification parameters (G, V) in directionally solidified Al–Cu alloys: this work

C_o (Al–wt.% Cu)	G (K mm^{-1})	V (μm s^{-1})	λ_1 (μm)	λ_2 (μm)	R (μm)	d (μm)	Relationships
3	1	8	750 ± 90	77 ± 2	67 ± 3	16,200 ± 750	
	2	8.5	590 ± 20	70 ± 2	51 ± 2	13,200 ± 650	$\lambda_1 = k_1 G^{-0.41}$
	2.7	10	465 ± 25	62 ± 1	44 ± 2	11,800 ± 500	$\lambda_1 = k_2 V^{-0.32}$
	4.1	9.5	410 ± 15	53 ± 4	36 ± 3	9100 ± 450	$\lambda_2 = k_3 G^{-0.39}$
	5.5	9	390 ± 35	38 ± 2	27 ± 3	7200 ± 400	$\lambda_2 = k_4 V^{-0.46}$
	5.5	19	325 ± 35	33 ± 3	21 ± 2	6900 ± 450	$R = k_5 G^{-0.51}$
	5.5	50	250 ± 20	21 ± 2	14 ± 1	6000 ± 400	$R = k_6 V^{-0.60}$
	5.5	90	180 ± 15	17 ± 1	10 ± 1	4900 ± 350	$d = k_7 G^{-0.47}$
	5.5	185	145 ± 15	12 ± 1	5 ± 0.5	3500 ± 300	$d = k_8 V^{-0.30}$
	5.5	490	115 ± 10	6 ± 0.5	2.5 ± 0.2	2200 ± 300	
6	1.6	8.5	820 ± 10	88 ± 6	91 ± 4	29,400 ± 1500	
	2.4	9	650 ± 20	62 ± 6	79 ± 4	25,800 ± 1400	$\lambda_1 = k_9 G^{-0.57}$
	3.6	9	520 ± 20	55 ± 5	61 ± 4	23,400 ± 1400	$\lambda_1 = k_{10} V^{-0.28}$
	4.6	9	450 ± 25	45 ± 3	48 ± 3	18,800 ± 1350	$\lambda_2 = k_{11} G^{-0.62}$
	5.7	9	395 ± 25	38 ± 2	34 ± 2	16,200 ± 1300	$\lambda_2 = k_{12} V^{-0.32}$
	5.7	18	315 ± 25	28 ± 3	19 ± 2	13,800 ± 1200	$R = k_{13} G^{-0.74}$
	5.7	45	245 ± 15	23 ± 2	15 ± 1	11,400 ± 900	$R = k_{14} V^{-0.56}$
	5.7	95	215 ± 20	18 ± 1	9 ± 0.5	9200 ± 700	$d = k_{15} G^{-0.46}$
	5.7	170	165 ± 10	15 ± 1	6 ± 0.5	7200 ± 500	$d = k_{16} V^{-0.35}$
	5.7	470	130 ± 10	10 ± 1	3.5 ± 0.2	3800 ± 200	
15	1.4	8	625 ± 30	66 ± 4	36 ± 3	19,000 ± 1200	
	2.6	11	510 ± 40	59 ± 3	26 ± 2	15,100 ± 1000	$\lambda_1 = k_{17} G^{-0.43}$
	3.4	9.5	421 ± 30	43 ± 4	19 ± 2	12,300 ± 850	$\lambda_1 = k_{18} V^{-0.23}$
	5.1	8	370 ± 20	39 ± 2	16 ± 1	9600 ± 700	$\lambda_2 = k_{19} G^{-0.48}$
	6.4	9	325 ± 30	32 ± 2	13 ± 1	7600 ± 550	$\lambda_2 = k_{20} V^{-0.39}$
	6.4	17	295 ± 25	26 ± 2	9 ± 1	7000 ± 450	$R = k_{21} G^{-0.67}$
	6.4	45	260 ± 20	21 ± 2	7 ± 0.5	6300 ± 400	$R = k_{22} V^{-0.43}$
	6.4	85	210 ± 15	14 ± 0.5	4 ± 0.3	5400 ± 450	$d = k_{23} G^{-0.60}$
	6.4	175	180 ± 15	11 ± 0.5	3.5 ± 0.2	4100 ± 400	$d = k_{24} V^{-0.21}$
	6.4	430	130 ± 10	7 ± 0.5	2.5 ± 0.2	3400 ± 300	
24	1.4	10	640 ± 20	60 ± 6	42 ± 1	11,200 ± 800	
	2.4	11	525 ± 20	47 ± 7	29 ± 1	9500 ± 700	$\lambda_1 = k_{25} G^{-0.30}$
	4.3	12	470 ± 35	28 ± 2	24 ± 2	7700 ± 650	$\lambda_1 = k_{26} V^{-0.29}$
	6.6	10	425 ± 40	22 ± 2	15 ± 1	5400 ± 450	$\lambda_2 = k_{27} G^{-0.70}$
	7.4	10	360 ± 35	19 ± 1	12 ± 1	3800 ± 300	$\lambda_2 = k_{28} V^{-0.27}$
	7.4	18	330 ± 20	15 ± 1	9 ± 0.5	3200 ± 200	$R = k_{29} G^{-0.70}$
	7.4	40	280 ± 20	13 ± 1	7 ± 0.5	2500 ± 150	$R = k_{30} V^{-0.39}$
	7.4	90	220 ± 20	10 ± 1	5 ± 0.2	2100 ± 100	$d = k_{31} G^{-0.58}$
	7.4	195	180 ± 10	8 ± 1	4 ± 0.3	1800 ± 150	$d = k_{32} V^{-0.25}$
	7.4	490	120 ± 10	6 ± 0.5	2.5 ± 0.3	1400 ± 100	

λ_1, Obtained from average values of the area counting method and the triangle method (see Appendix A).

capable of recording to 1 μV. Temperature of all the thermocouples were recorded during the run.

Temperature of the second thermocouple at the solid–liquid interface and then third thermocouple in the liquid were recorded simultaneously for measurement of the temperature gradients on the solid/liquid interface in the liquid. The position of the thermocouples were measured after the quench. Cooling water level (with the constant temperature) was always kept at the same position in order to check the furnace temperature. Thus, the sample temperature was constant. The temperature gradient can be changed by changing the sample temperature and/or the distance between the cooling water level and the hot stage. G can be kept constant during the run because the temperature of the cooler and the hotter part of the furnace and the distance between them were constant.

It was found that the pulling speed was similar to the growth rates; this may be due to the metal sample holder and the graphite crucible which have good thermal conductivity. The growth rate was calculated with two different methods. In the first method, the values for the growth rate were calculated from the measurements of the time taken for the solid/liquid interface to pass the thermocouples separated by a known distance. In the second method, solidification time and solidification distance (on the longitudinal section of the polished sample) were measured. The ratio of the distances to the times were measured to obtain the growth rates and these were similar for both methods.

2.2. Metallographic examination

The unidirectionally grown quenched specimen was removed from the graphite crucible, then ground to observe the solid–liquid interface and the longitudinal section which included the quenched interface which was separated from the specimen. This part was ground, polished and etched to reveal the quenched interface. Furthermore, the longitudinal and the transverse sections of the ground specimen were cold-mounted with epoxy-resin. The microstructural of the specimen was determined by metallographic analysis. Mechanical and electropolishing techniques were used to prepare the transverse and the longitudinal sections for both optical microscopy (OM) and scanning electron microscopy (SEM).

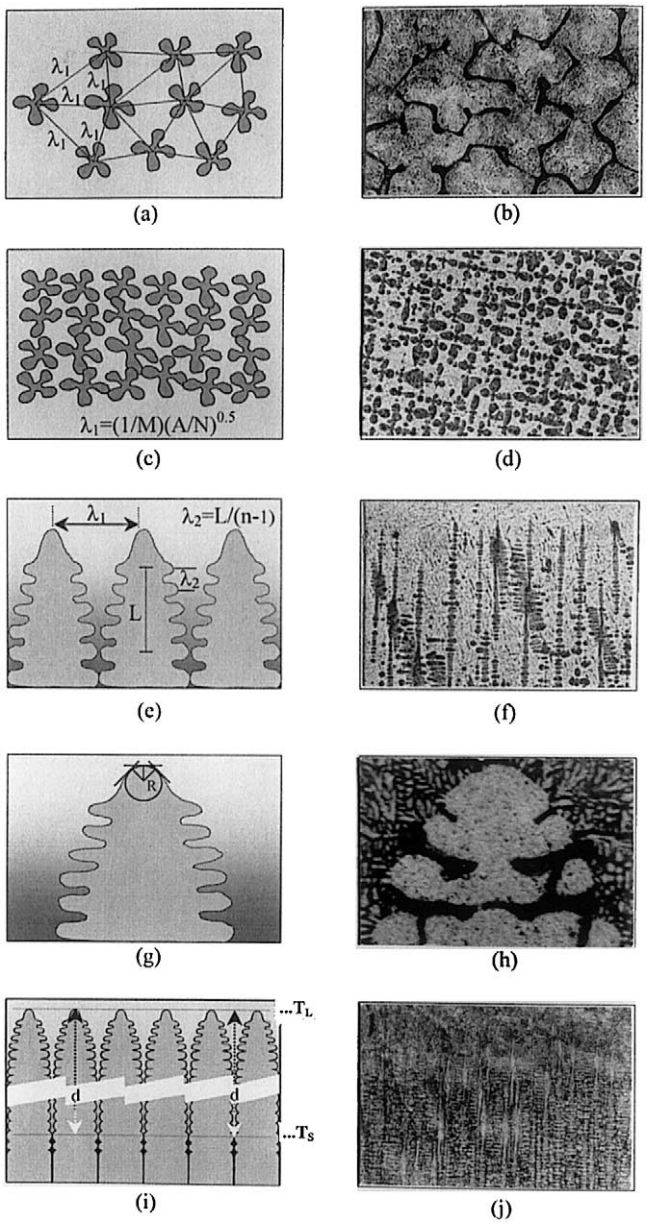

Fig. 2. Microstructural parameters and measurement pocedure, diagram and picture of: (a), (b) triangle method, (c), (d) area counting method (M: magnification factor, A: total area, N: number of primary dendrites), (e), (f) intercept method (L: length, n: number of secondary arms), (g), (h) dendrite tip radius R, (i), (j) mushy zone depth d.

2.3. Measurement of primary dendrite arm spacing

The λ_1 values measured on the transverse section (perpendicular to the growth direction) Fig. 2(a)–(d) gave more accurate results than the λ_1 values measured on the longitudinal section (parallel to the growth direction). Two different methods were used for measurement of the primary dendrite arm spacings on the transverse sections. The first method is the triangle method [82]. The triangle occurred by joining the three neighbor dendrite centers and sides of the triangle corresponded to λ_1 (see Fig. 2(a)). In this method at least 50–400 λ_1 values were measured for each specimen. The second method is the area counting method [1,5,8,9,82,83]. In this method, λ_1 values were measured on the crossection, at least on four different regions for each specimen (see Fig. 2(c)). λ_1 is equal to $(1/M(A/N)^{0.5}$ where M is the magnification factor, A is the total specimen crossection area and N is the number of primary dendrites on the crossection. Depending on growth conditions, 50–400 λ_1 were observed and counted on the corresponding specimen crossections.

2.4. Measurement of secondary dendrite arm spacings

Values of λ_2 were measured by averaging the distance between adjacent side branches on the longitudinal section of a primary dendrite as a function of the distance from the dendrite tip as can be seen from Fig. 2(e) and (f). Each of the side-branch spacing data reported here is the average of the initial λ_2 values from 30 to 40 primary dendrites for each specimen.

2.5. Measurement of dendrite tip radius

The tip radius R was measured by fitting a suitable circle on the dendrite tip side as can be seen in Fig. 2(g) and (h). These measurements were repeated at least 15–20 times on dendrites for each G and V.

2.6. Measurement of mushy zone depth

The zone depth d is defined as the average distance between tip and root of the dendrites as can be seen in Fig. 2(i) and (j). This parameter was measured as far from steady state condition in the dendrites as possible and found to be the average value of these measurements. The measurements were repeated about 15–20 times for each specimen.

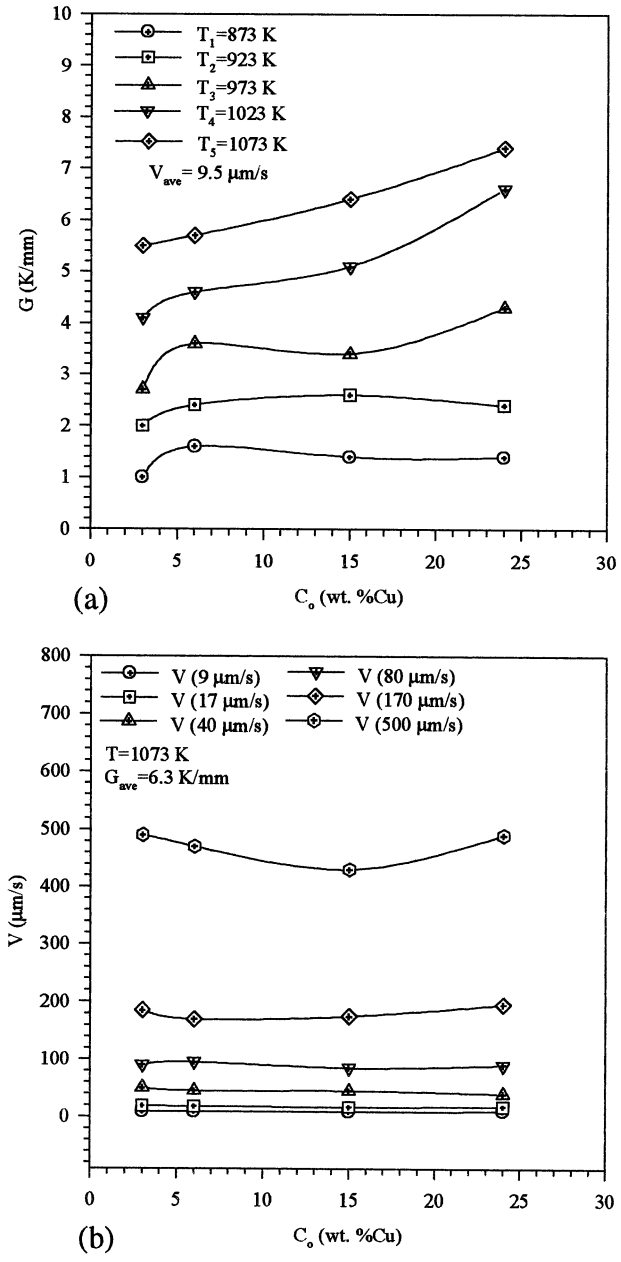

Fig. 3. (a) Composition effect on temperature gradients. (b) Composition effect on growth rates.

3. Result and discussion

The purpose of this work is to experimentally investigate the relationship between solidification parameters (G, V) and the microstructural parameters (λ_1, λ_2, R, d) and see the effect of composition C_o on microstructural parameters, but before examining the effect of C_o on the microstructural parameters it would be useful to see the effect of C_o on G and V. Thermal conductivity coefficients (K_L, K_S of the liquid and the solid phases, respectively) decrease with the increasing temperature for a given C_o. K_L and K_S also decrease with the increasing Cu content in Al–Cu alloys [84,85]. K_L is smaller than K_S and decreases more rapidly than K_S. Thus G increases with the increasing C_o at high temperature. The effect of C_o on G and V is shown in Fig. 3. As can be seen from Fig. 3(a) there is no composition effect on G when the sample temperature is about 100 K above the eutectic temperature T_E for Al–(6,15,24) wt.%Cu alloys for a constant V ($V = 9.5$ μm s^{-1}), but in general G increases with the increasing C_o at higher temperature. As can be seen from Fig. 3(b), V does not change by the variation of C_o.

For the purpose of convenient measurements, the samples were grown directionally 100–120 mm under the steady state growth condition and then they were quenched by pulling them rapidly into the water reservoir. Directionally grown uniform samples with the microscopic planar interface without any faulty structures were chosen in order to obtain reliable measurements for the microstructural parameters. To investigate the influence of solidification parameters (G,V) on the dendritic microstructure parameters (λ_1, λ_2, R and d) and see the effect of composition C_o, on the microstructural parameters, a series of forty experiments (ten experiments for each composition) were carried out with temperature gradients of 1.0–7.4 K mm^{-1} and growth rates of 9–490 μm s^{-1} for different Al–Cu alloys. Figs. 4–7 show longitudinal and transverse views of the specimen studied to examine the influence of microstructural parameters depending on solidification parameters.

3.1. Composition effect on the microstructural parameters

It has been shown that convection has an important effect on the microstructural parameters [6,8,86–88]. In order to eliminate or at least minimize convection in alloy specimens solidified vertically upwards, it is necessary, not only to have a hydrodynamical stable vertical density gradient, but also to have near zero horizontal density gradient. One way of doing this would be to maintain an absolute planar macroscopic solid-liquid interface at all times [89,90]. A planar macroscopic interface obtained by using a 4 mm diameter specimens. All the data can be obtained from the specimens with macroscopically planar interfaces. Experiments were run with Al–(3,6,15,24) wt.% Cu alloys and at a variety of G and V. These data are summarized in Table 1 and Figs. 8–15 for different Al–Cu alloys. Plotting of the experimental data on microstructural parameters as a function of alloy composition is not directly possible because the temperature gradients and the growth rates are not exactly alike for the various Al–Cu alloys. As can be seen from Fig. 3(a) the temperature

gradient is also affected by the alloy composition for the higher temperature. The effect of composition on microstructural parameters (except d) was found to be quite small for different G and V values (Table 1, Figs. 8–14). As can be seen from Fig. 15(b), d value increases with the increasing C_o until $C_o = 6$ wt.% Cu content and then decreases with the increasing C_o values. When $C_o = 0$ and $C_o = C_E$ d goes to zero because at these composition ΔT_o goes to zero as expected from the phase diagram (Fig. 1) and Eq. (11). As to be expected there is the same scattering of the points but in most alloy it is small and random. The effect of composition in a given system is generally within the bounds of experimental scattering in microstructural parameters.

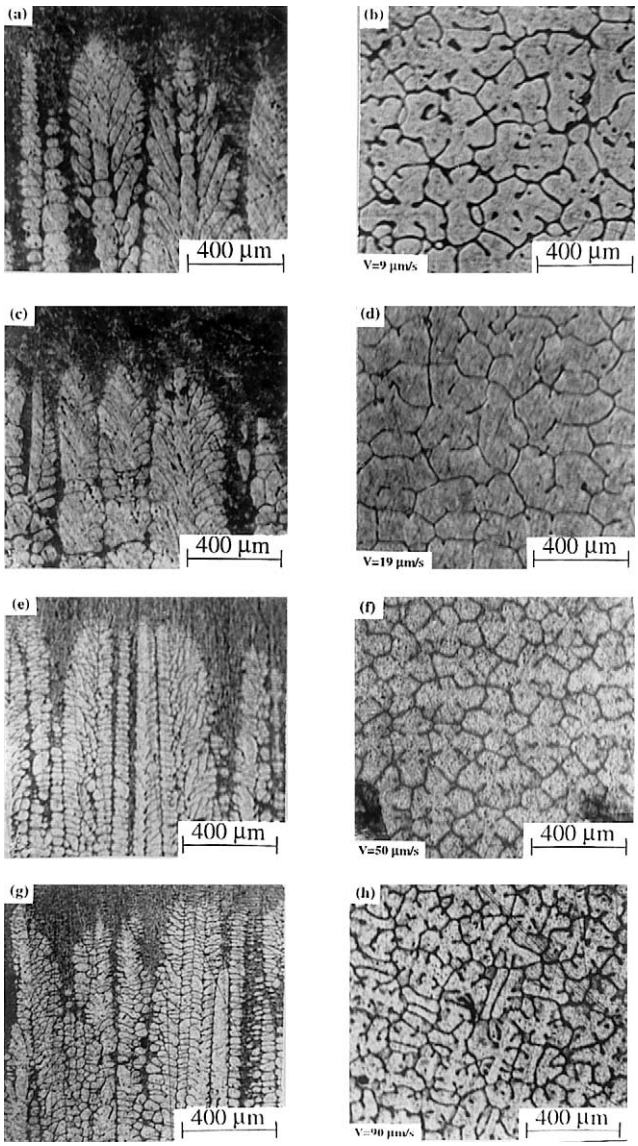

Fig. 4. Dendritic structures of directionally solidified Al–3 wt.% Cu alloy with constant G (5.5 K mm^{-1}) for different V. Longitudinal sections (a), (c), (e), (g), transverse sections (b), (d), (f), (h).

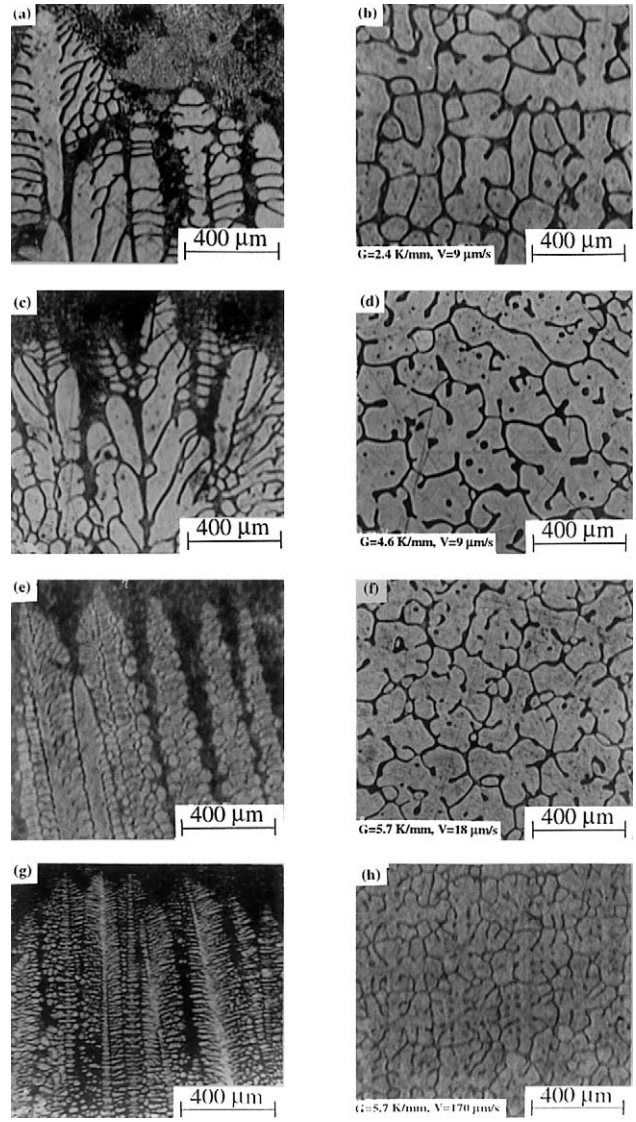

Fig. 5. Dendritic structures of directionally solidified Al–6 wt.% Cu alloy for different G and V. Longitudinal sections (a), (c), (e), (g), transverse sections (b), (d), (f), (h).

3.2. Primary dendrite arm spacing

One of the most important quantities used to describe dendritic microstructure in directional growth is the primary dendrite arm spacing. The photographs of the specimens on solidification parameters and microstructural parameters for unidirectionally solidified Al–Cu alloys are shown in Figs. 4–7 and the λ_1 values are given in Table 1. In order to determine λ_1 versus G, measurement of dendrite spacings were made over a range of temperature gradients at a constant velocity ($V \cong 9.5$ μm s^{-1}) for different Al–Cu alloys. The plots of the log λ_1 versus log G data obtained at constant velocity are shown in Fig. 8(a) for the Al–Cu alloys. As can be seen from Fig. 8(a), the data form a family of straight lines. Thus, we can describe the mathematical

relationship between λ_1 and G by linear regression analysis for each composition as $\lambda_1 = k_1 G^{-a1}$. It is apparent that λ_1 changed inversely proportional to G (Fig. 8(a)). However, the gradient exponents a_1 of this family of the lines are not equal, but decrease systematically with C_o except Al–3 wt.% Cu alloy. The value of the gradient exponents a_1 depend on C_o and equal to 0.41, 0.57, 0.43 and 0.30 for the Al–(3, 6, 15, 24)wt.% Cu alloys, respectively, ($\bar{a}_1 = 0.43 \pm 0.10$). Our detailed experimental studies show that the λ_1 values decrease with the increasing G. Such variation in λ_1 has also been found in a number of other systems, especially in Al–4.5 wt.% Cu alloy by Su et al. [54], in Pb–(5–95) wt.% Sn alloys by Çadırlı et al. [55], in Pb–19 wt.% Sn alloy by Klaren et al. [9], in Al–(9.5–28.1) wt.% Fe

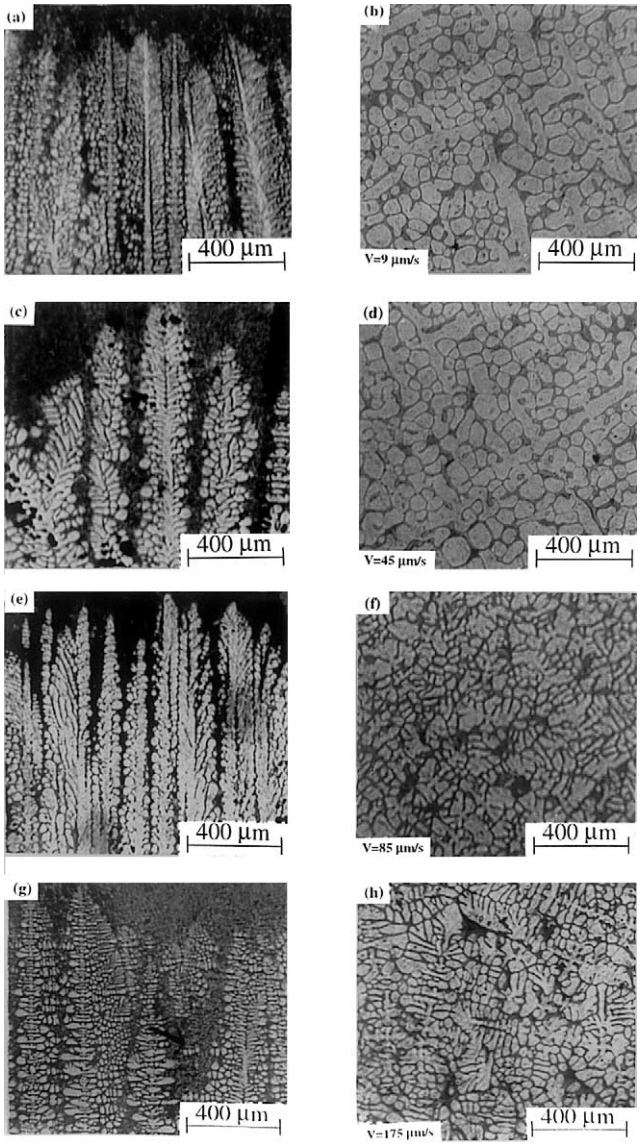

Fig. 6. Dendritic structures of directionally solidified Al–15 wt.% Cu alloy with constant G (6.4 K mm^{-1}) for different V. Longitudinal sections (a), (c), (e), (g), transverse sections (b), (d), (f), (h).

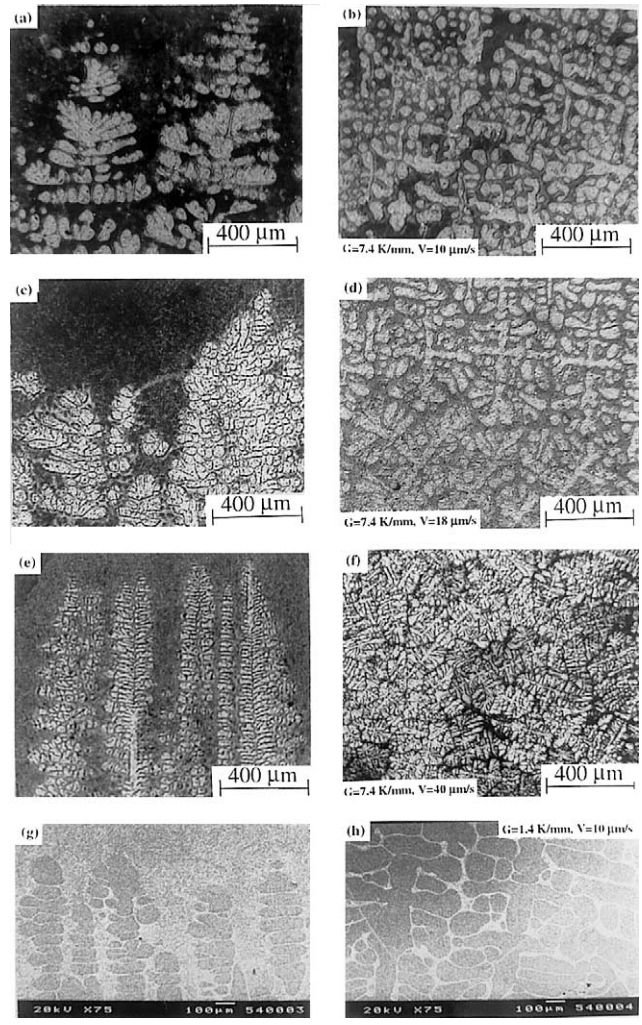

Fig. 7. Dendritic structures of directionally solidified Al–24 wt.% Cu alloy for different G and V. Longitudinal sections (a), (c), (e), (g), transverse sections (b), (d), (f), (h).

alloys by Liang et al. [11], in Zn–8 wt.% Al alloy by Tunca and Smith [56], in Fe–(1.48 wt.% C–1.14 wt.% Mn) alloy by Jacobi and Schwerdtfeger [57].

Variation in λ_1 with V at the constant G for different Al–Cu alloys are shown in Fig. 8(b) and Table 1. The variation of λ_1 on the log λ_1 versus log V plot is essentially linear for the growth rates between 9 and 490 μm s^{-1}. It can be seen that the points fall on a family of straight lines each corresponding to a C_o (Fig. 8(b)). A linear regression analysis gives the proportionality equation as $\lambda_1 = k'_1 V^{-b1}$. Fig. 8(b) shows clearly that an increase in V produce a decrease in λ_1. The value of the growth rate exponent b_1 is equal to 0.32, 0.28, 0.23 and 0.29 for the Al–(3, 6, 15, 24) wt.% Cu alloys respectively, ($\bar{b}_1 = 0.28 \pm 0.03$). The value of the growth rate exponent b_1 is found not to vary with C_o. The dependence of λ_1 on V was studied over a composition range of 3–24 wt.% Cu, and in this range, no significant effect was observed on either the exponent b_1

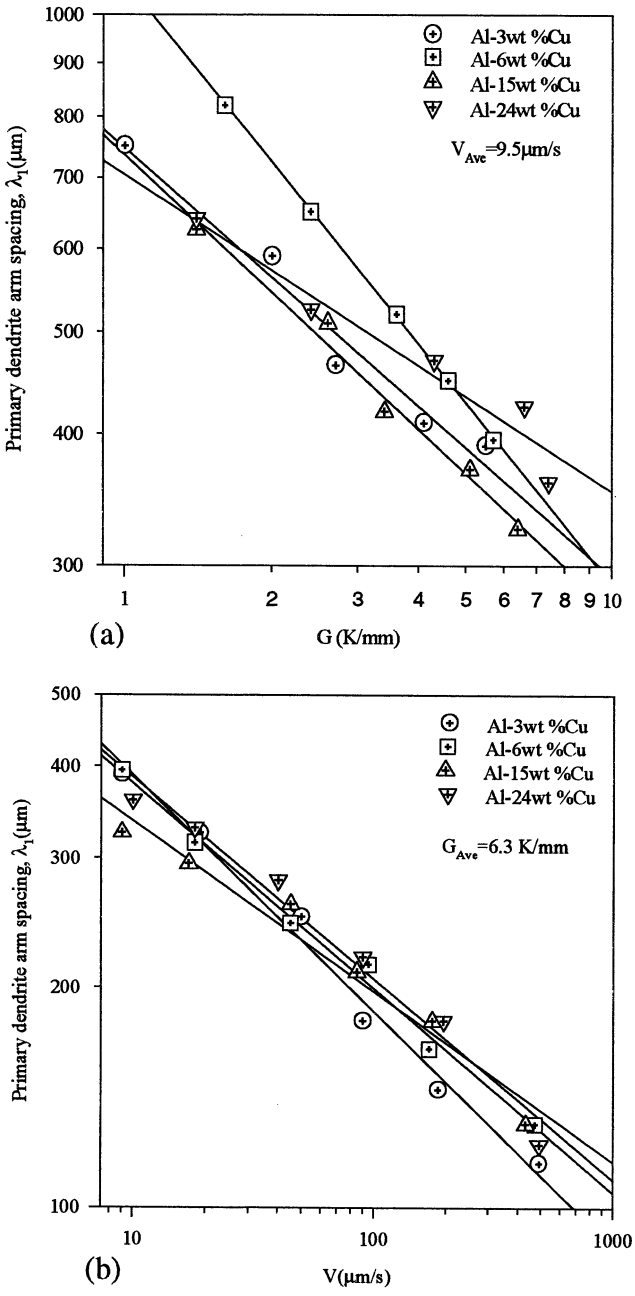

Fig. 8. (a) Variation of λ_1 with G at constant V for different Al–Cu alloys. (b) Variation of λ_1 with V at constant G for different Al–Cu alloys.

or the proportionality constant k'_1 of the relation $\lambda_1 = k'_1 V^{-b1}$ (see Appendix A). In general the effects of composition on λ_1 is small.

A number of experimental studies have been reported in the literature to characterize the variation in the λ_1 with V (see Table 2). The relationships obtained between λ_1 and V for Al–(6,15,24) wt.% Cu alloys are in good agreement with the relationships obtained by Taha [53] with similar composition. A decrease in λ_1 with V was observed in Al–Cu alloys by the different researchers [3–7,36,52–54], in Pb–Sn alloys by the other works [8,9,55], in Pb–8 wt.% Au alloy by Klaren et al. [9], in Al–11 wt.% Mg alloy by Liu and Kang [10], in Zn–Al alloys by Tunca and Smith [56], in Ni base superalloy by Kermanpur et al.[12], in succinonitrile–2.5 wt.% ethanol by Huang et al. [13] and succinonitrile–acetone system by Trivedi and Somboonsuk [41] and by Esaka and Kurz [63]. Examination of the data of Tables 1 and 2 show that the gradient exponent a_1 varies between 0.32 and 0.72, but mostly closer to 0.5 and the growth rate exponent b_1 varies between 0.24 and 0.50, but mostly closer to 0.3. Experimental studies carried out in different systems either metallic [3–13,32,52–57] or organic [13,43,63] showed a slight variation of the exponent a_1 and b_1 on the particular alloy system and the alloy composition used.

The comparison of the experimentally obtained λ_1 with the calculated λ_1 by the Hunt model [38], the Trivedi model [40], the Kurz–Fisher model [39] and the Hunt–Lu model [33] are given in Fig. 9 (physical parameters of Al–Cu alloys used in λ_1 calculations for the models are given in the Appendix B). The λ_1 values calculated by the Kurz–Fisher model for all compositions were too large when compared with our experimental results (Fig. 9(a)–(d)). The lines obtained from the Trivedi model lies slightly above the experimental line while the ones from the Hunt model slightly below the experimental one. The experimental λ_1 values were in good agreement with the λ_1 values calculated by the Trivedi model for Al–(3.6) wt.% Cu alloys (Fig. 9(a), (b)). Whereas, the λ_1 values obtained by the Hunt model agrees very well with the experimental λ_1 values for Al–(15,24) wt.% Cu alloys. The numerical model presented by Hunt and Lu [33] is also used to calculate λ_1 as a function of V for given C_o and G and compares with the experimentally determined λ_1 values in Fig. 9(e). The experimental results are in quite good agreement with the calculated Hunt–Lu model, especially for Al–(3,6,15) wt.% Cu alloys for the growth rates between 20–200 μm s^{-1}. Significant discrepancies are noticed between experimental and the calculated values for growth rates smaller than 20 μm s^{-1} for higher alloy compositions (Al–(15,24) wt.% Cu), and for growth rates higher than 200 μm s^{-1} for lower alloy compositions (Al–(3,6) wt.% Cu).

It was found that the experimental λ_1 values and calculated λ_1 values decrease for high growth rates ($V > V_{cs}/k$) for Al–Cu alloys (Fig. 9). Similar results were obtained by the other studies [15–17,19,58,91,92]. We compared the results obtained on the transparent model alloy systems to demonstrate this conclusion further [13,43,63].

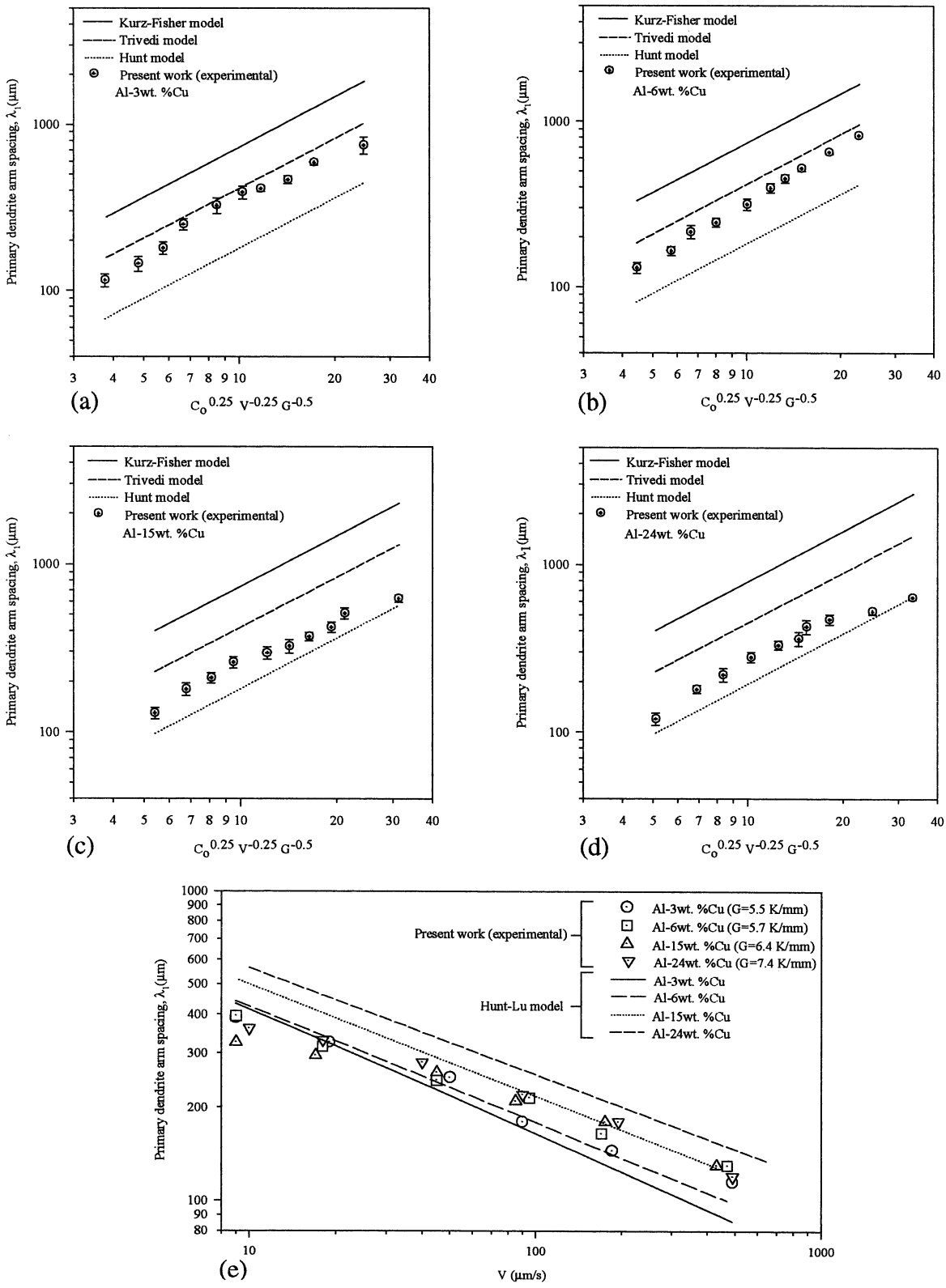

Fig. 9. Comparison of λ_1 obtained with experimental work and λ_1 obtained with theoretical models [38–40] for different Al–Cu alloys. (a) Al–3 wt.% Cu, (b) Al–6 wt.% Cu, (c) Al–15 wt.% Cu, (d) Al–24 wt.% Cu, (e) the results of the experimental work and the Hunt–Lu numerical model [33].

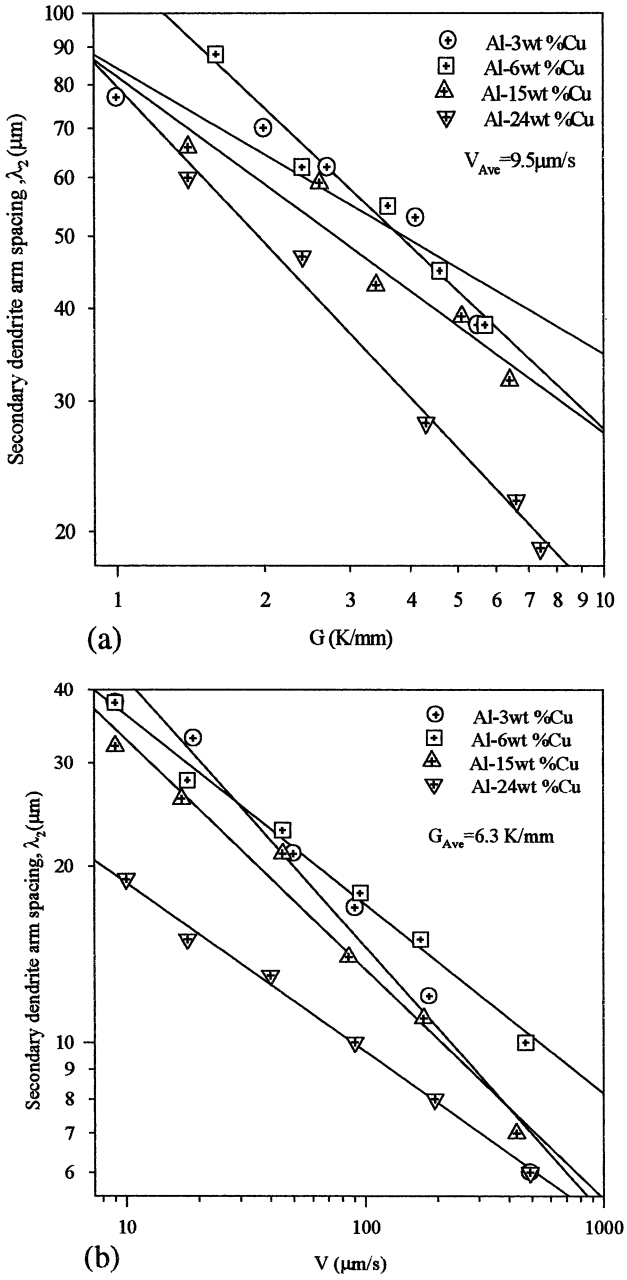

Fig. 10. (a) Variation of λ_2 with G at constant V for different Al–Cu alloys. (b) Variation of λ_2 with V at constant G for different Al–Cu alloys.

3.3. Secondary dendrite arm spacing

The λ_2 values were measured in the usual manner on the longitudinal sections by counting the number of arms over a certain length of primary arm axis, and the measurement of λ_2 and R were made on the same dendrite for each run. The variation in λ_2 with G at constant V for the different Al–Cu alloys are shown in Fig. 10(a) and Table 1. Fig. 10(a) shows that an increase in G cause a decrease in λ_2. A linear regression

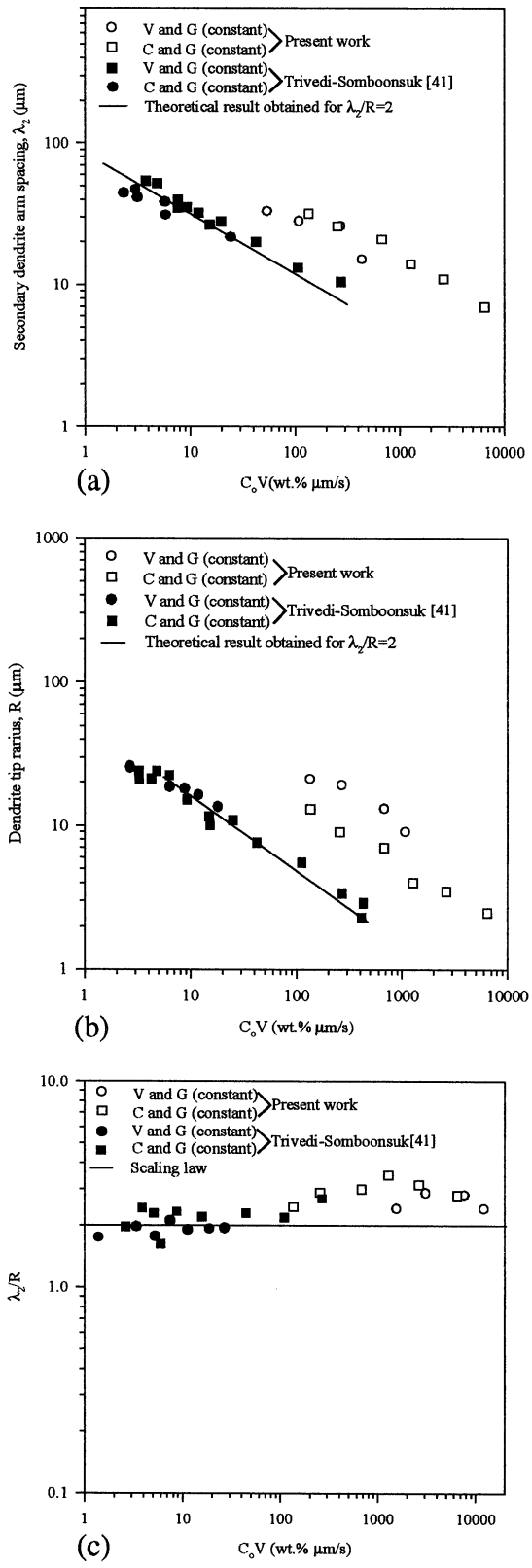

Fig. 11. (a) Variation of λ_2 with C_oV at constant G (6.3 K mm^{-1}). (b) Variation of R with C_oV at constant G (6.3 K mm^{-1}). (c) Variation of λ_2/R with C_oV at constant G (6.3 K mm^{-1}) and comparison of the result with the scaling law.

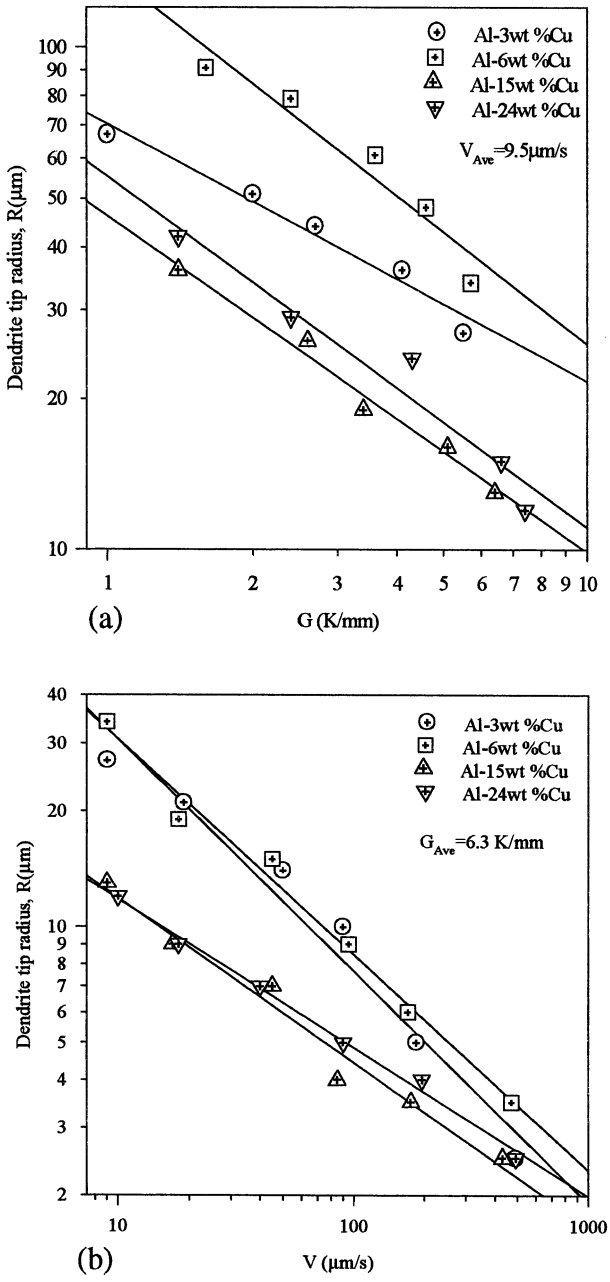

Fig. 12. (a) Variation of R with G at constant V for different Al–Cu alloys. (b)Variation of R with V at constant G for different Al–Cu alloys.

analysis gives the proportionality equation as $\lambda_2 = k_2 G^{-a2}$. The value of the gradient exponent a_2 for λ_2 equals to 0.39, 0.62, 0.48 and 0.70 for the Al–(3,6,15,24) wt.% Cu alloys, respectively (see Table 1). The relationship obtained between λ_2 and G in this work for Al–(6,15) wt.% Cu alloys are in good agreement with the relationship obtained by Jacobi and Schwerdtfeger [57] with the Fe–(1.48 C–1.14 Mn) wt.% alloys. The relationships obtained between λ_2 and G in this work with Al–(3,24) wt.% Cu alloys are also in good agreement with the relationships obtained by Çadırlı et al. [55] with the Pb–(5–95) wt.% Sn alloys.

The present work revealed that the relationship between λ_2 and V at constant G in the Al–Cu alloys can be represented by the empirical equation $\lambda_2 = k'_2 V^{-b2}$ for the range of V used (Fig. 11(b) and Table 1). The value of the growth rate exponent b_2 equals to 0.46, 0.32, 0.39 and 0.27 for the Al–Cu alloys studied ($\bar{b}_2 = 0.36 \pm 0.07$). The dependence of λ_2 in relationship to G and V are approximately the same for Al–(3,6) wt.% Cu alloys. On the other hand, the value of the exponent a_2 is twice higher than the exponent b_2 in Al–(6,24) wt.% Cu alloys. The relationships obtained between λ_2 and V in this work with Al–(6,24) wt.% Cu alloys give similar results with the relationships obtained by Taha [53] with the Al–5.7 wt.% Cu alloys and by Liu and Jones [75,76] with the Zn–Mg alloys (Tables 1 and 2). The dependence of λ_2 with V obtained by Tunca and Smith [56] with Zn–Al alloys, by Jacobi and Schwerdtfeger [57] with Fe–(1.48 C–1.14 Mn) wt.% alloys are also similar to our experimental relationships obtained with Al–(3,15) wt.% Cu alloys (Table 1). The data on other alloys found in the literature indicated values for b_2 of 1.08 in Pb–(5–10) wt.% Sb alloys by Kottler et al. [93], and 0.56 in succinonitrile–5.5 mol acetone alloys by Somboonsuk et al. [43].

The effect of C_oV on λ_2 and R are shown in Fig. 11 (a)–(b) and Appendix A, for the present results as well as those of theoretical [62] and Trivedi–Somboonsuk results [41] as a log–log plot. It is apparent that the λ_2 and R values decrease with the increase of C_oV. Variation of λ_2 with C_oV at constant G can be represented by the empirical equation as $\lambda_2 = k(C_oV)^{-0.32}$ and the variation of R with C_oV at constant G can be represented as $R = k'(C_oV)^{-0.43}$, which is in good agreement with the results of Sharp and Hellawell [4] for the similar Al–Cu alloys. Fig. 11(c) shows the ratio λ_2/R as a function of C_oV. No clear effect of C_oV on this ratio has been observed. The value of λ_2/R for the C_oV range studied in this work is 2.8 ± 0.4. This value is approximately equal to the value found by Huang and Glicksman [64] as a definite scaling law exists between λ_2 and R, $\lambda_2/R = 3.0$. As can be seen from Fig. 11(c), our experimental results are in good agreement with the results of the scaling law and the results of Trivedi and Somboonsuk [41]. Langer [94] and Müller-Krumbhaar and Langer [95] have estimated that λ_2/R should be equal to 2.1 for undercooled dendrites in pure substances. The ratio λ_2/R was found to be 2.0 in succinonitrile–4 wt.% acetone system by Trivedi and Somboonsuk [41], whereas a value of 2.5 was found for thermal dendrites in pure succinonitrile and 3.8 in the Pivalic acid–ethanol system [96]. The value of the scaling factors was found to be 3.18 and 3.47 for the CBr_4 and C_2Cl_6 system respectively [45]. Similarly Honjo and Sawada [65] reported $\lambda_2/R = 4.68$ for the

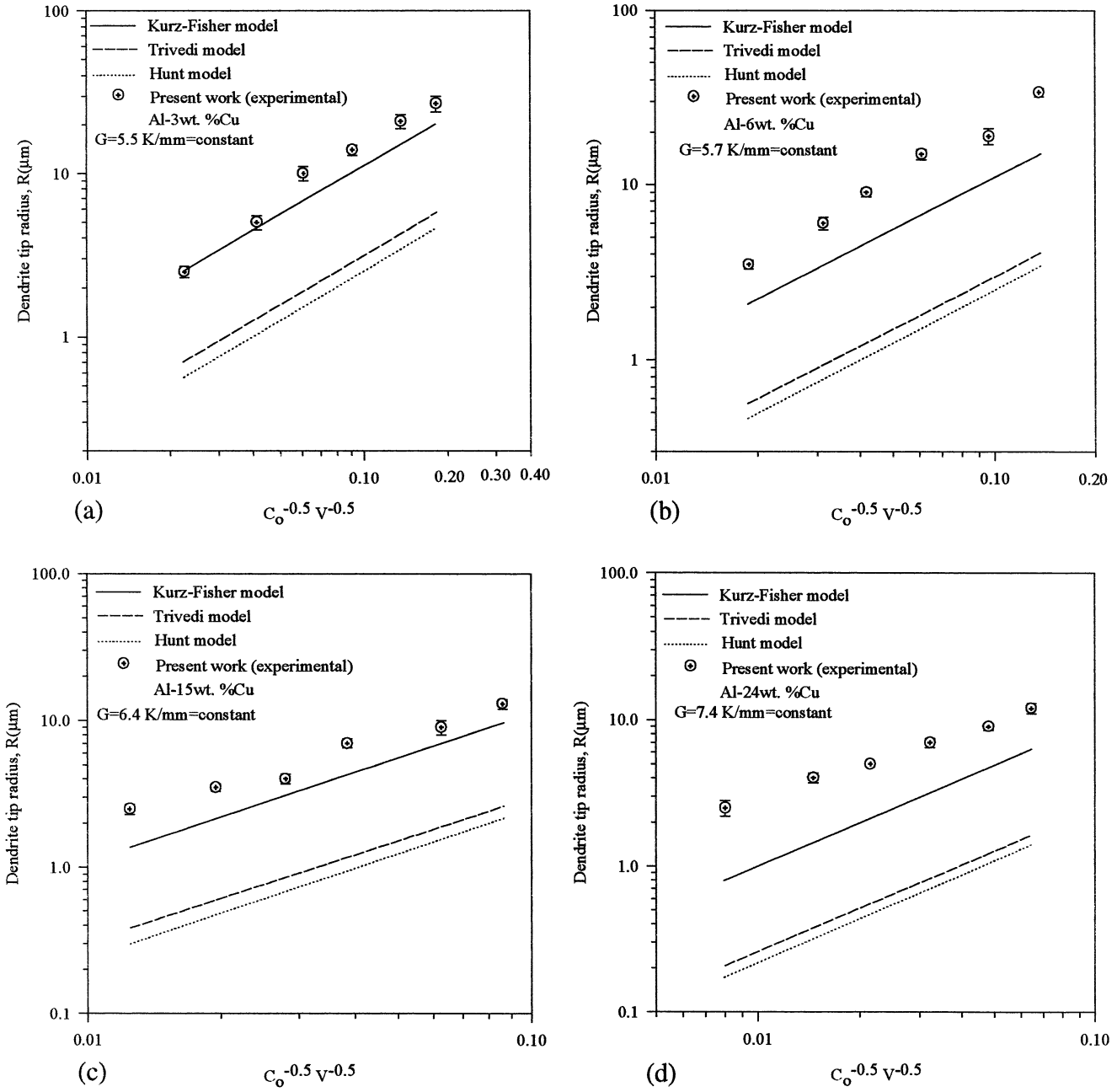

Fig. 13. Comparison of R obtained with experimental work and R obtained with theoretical models [38–40] for different Al–Cu alloys. (a) Al–3 wt.% Cu, (b) Al–6 wt.% Cu, (c) Al–15 wt.% Cu, (d) Al–24 wt.% Cu.

growth of the dendrites in an undercooled water–NH_4Br solution. It appears that an increase in anisotropy cause an increase in λ_2/R value. The value of λ_2/R seems to depend on the experimental conditions which give rise to the value of the constant.

As a matter of cause, λ_2 can be investigated as a function of the local solidification time t_f [97–102]. As mentioned above the main purpose of this work is to investigate the microstructural parameters (λ_1, λ_2, R, d) as function of solidification parameters (G, V, C_o); thus, we believe that examining of λ_2 as function of t_f should be out of the scope of this work.

3.4. Dendrite tip radius

The plot of log R versus log G data obtained at the constant V and log R versus log V data obtained at the constant G are shown in Fig. 12 and Table 1 for the Al–Cu alloys. As can be seen from Fig. 12(a), the data form a family of straight lines. Thus the mathematical relationship between R and G can be described as $R = k_3 G^{-a3}$. It is clear that R changes inversely proportional to G (see Fig. 12(a) and Table 1). The gradient exponent a_3 for R equal to 0.51, 0.74, 0.67 and 0.70 for the Al–(3, 6, 15, 24) wt.% Cu alloys respectively.

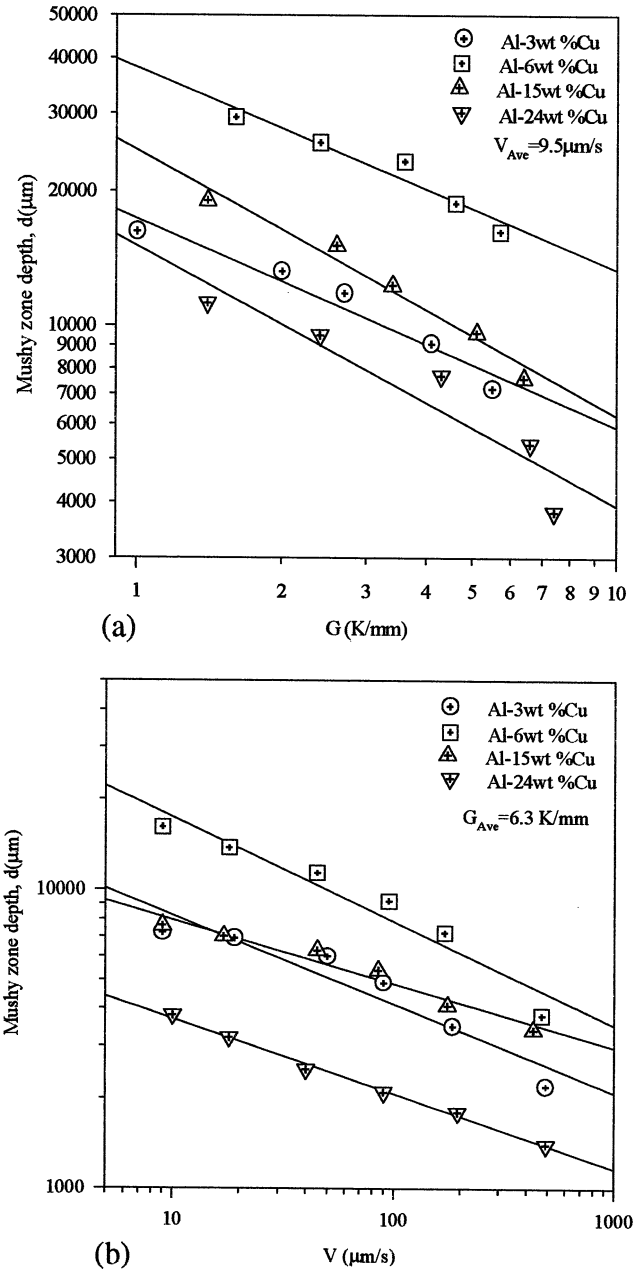

Fig. 14. (a) Variation of d with G at constant V for different Al–Cu alloys. (b) Variation of d with V at constant G for different Al–Cu alloys.

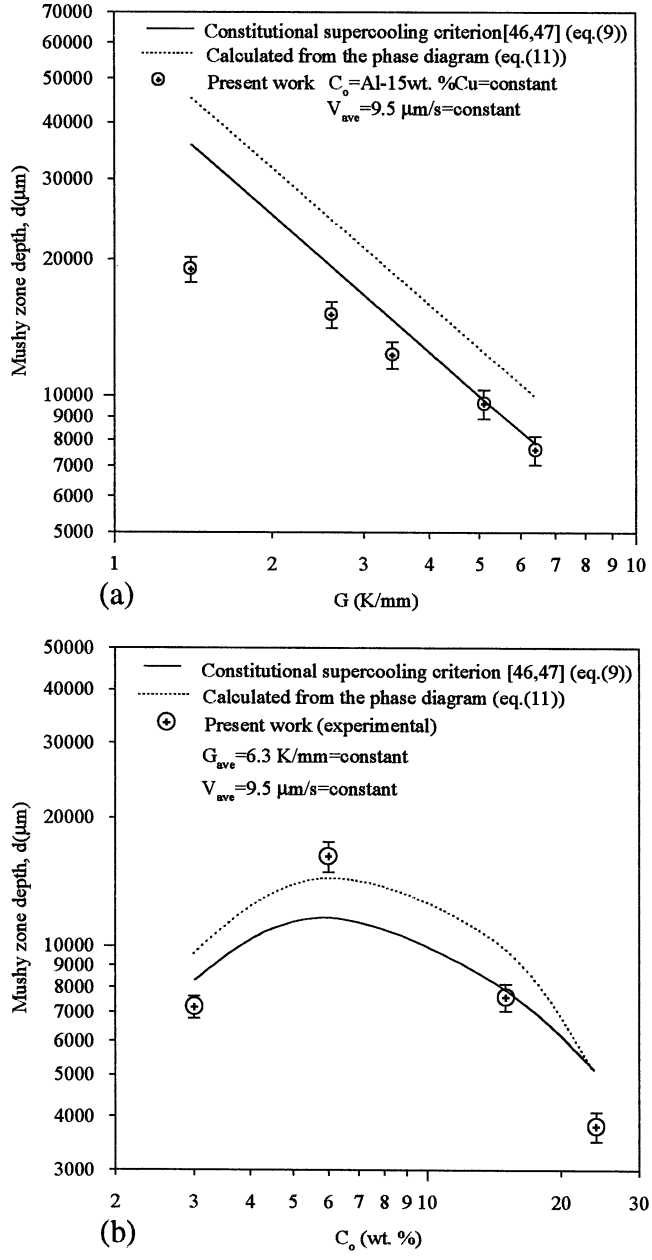

Fig. 15. Variation of the experimental and predicted d values, (a) with G for Al–15 wt.% Cu alloy at constant V, (b) with C_o at constant G and V.

As can be seen from Fig. 12(b) and Table 1, R decreases with the increasing V according to $R = k'_3 V^{-b3}$ for the constant G for given alloy compositions. Here R is proportional to V of a power of -0.60, -0.56, -0.43 and -0.39 for Al–(3,6,15,24) wt.% Cu alloys, respectively ($\bar{b}_3 = 0.50 \pm 0.09$). These are in quite good agreement with the theoretical predictions [38–40]. The value of the exponent b_3 seems to decrease with the increasing C_o. The exponent values of a_3 is higher than the exponent value of b_3 for Al–(6,15,24) wt.% Cu alloys. It appears that the dependence of R on G is more sensitive than the dependence of R on V. The relationships obtained between R and V in this work for Al–(3,6,15) wt.% Cu alloys are in good agreement with the relationships obtained by Miyata et al. [36] with Al–(4.8–49.8) wt.% Cu alloys and the relationship obtained by Cattaneo et al. [42] with succinonitrile–1.3wt.% acetone solution (see Table 2).

Predictions of R by the theoretical models [38–40] are shown in Fig. 13 with the experimental data. The experimental results obtained in Al–(3,15) wt.% Cu alloys for R were in good agreement with the results

Table 2
Variation of microstructural parameters (λ_1, λ_2, R) with solidification parameters (G, V) for different metallic and organic materials: previous work

Composition	G (K mm^{-1})	V (μm s^{-1})	GV (K s^{-1})	Relationships	Ref.
Al–2 wt.% Cu	9.9	9.8–51.6	0.097–0.51	$\lambda_1 = k_1 G^{-0.54}$	[3]
Al–4.5 wt.% Cu	8.0	5.8–38.1	0.046–0.30	$\lambda_1 = k_2 V^{-0.28}$	
Al–2 wt.% Cu	7.5	30–440	0.22–3.3	$\lambda_1 = k_3 V^{-0.50}$	[4]
Al–2.4 wt.% Cu				$\lambda_1 = k_4 G^{-0.50} V^{-0.50}$	[52]
Al–4.4 wt.% Cu	0.8–10	50–500	0.04–5	$\lambda_1 = k_5 G^{-0.50} V^{-0.36}$	
Al–10.1 wt.% Cu				$\lambda_1 = k_6 G^{-0.50} V^{-0.43}$	
Al–4.1 wt.% Cu	4	0.2–70	0.0008–0.28	$\lambda_1 = k_7 V^{-0.40}$	
				$R = k_8 V^{-0.54}$	[36]
Al–(5.7–20) wt.% Cu	9	8–360	0.072–3.24	$\lambda_1 = k_9 V^{-0.36}$	[53]
				$\lambda_2 = k_{10} V^{-0.29}$	
Al–6 wt.% Cu	2.05–13.9	16.7–1000	0.034–13.9	$\lambda_1 = k_{11} G^{-0.55} V^{-0.28}$	[5]
Al–40 wt.% Cu	3	4.2–42	0.012–0.12	$\lambda_1 = k_{12} V^{-0.32}$	[6]
Al–4.5 wt.% Cu	8.8	10–240	0.088–2.11	$\lambda_1 = k_{13} V^{-0.38}$	[7]
Al–4.5 wt.% Cu	3.1	20–500	0.0062–1.55	$\lambda_1 = k_{14} (GV)^{-0.27}$	[54]
				$\lambda_2 = k_{15} (GV)^{-0.35}$	
Al–(2–20) wt.% Cu	7.5–16	6–33	0.042–0.53	$R = k_{16} (CV)^{-0.50}$	[66]
				$\lambda_1 = k_{17} G^{-n}$ ($n = 0.32$–0.71)	[55]
				$\lambda_1 = k_{18} V^{-n}$ ($n = 0.29$–0.40)	
Pb–(5–95) wt.% Sn	0.8–5.5	7–467	0.016–2.72	$\lambda_2 = k_{19} G^{-n}$ ($n = 0.50$–0.82)	
				$\lambda_2 = k_{20} V^{-n}$ ($n = 0.34$–0.49)	
Pb–40 wt.% Sn	10.7	45–400	0.48–4.28	$\lambda_1 = k_{21} V^{-0.39}$	[8]
Pb–19 wt.% Sn	1.1–37	20	0.022–0.74	$\lambda_1 = k_{22} G^{-0.32}$	[9]
Pb–8 wt.% Au	40	2–407	0.08–16.28	$\lambda_1 = k_{23} V^{-0.44}$	
Al–11 wt.% Mg	–	–	0.5–1	$\lambda_1 = k_{24} (GV)^{-0.33}$	[10]
Al–(9.5–28.1) wt.% Fe	1–13	10–6400	0.01–83.2	$\lambda_1 = k_{25} G^{-0.5} V^{-0.25}$	[11]
Zn–6.5 wt.% Al	7.5–10.5	10–1000	0.075–10.5	$\lambda_1 = k_{26} V^{-m}$ ($m = 0.25$–0.27)	[56]
				$\lambda_2 = k_{27} V^{-m}$ ($m = 0.32$–0.38)	
Zn–8 wt.% Al	7.5–12	10–1000	0.075–12	$\lambda_1 = k_{28} V^{-m}$ ($m = 0.24$–0.29)	
				$\lambda_2 = k_{29} V^{-m}$ ($m = 0.32$–0.42)	
Zn–11 wt.% Al	7.5–12	10–1000	0.075–12	$\lambda_1 = k_{30} V^{-m}$ ($m = 0.25$–0.30)	
				$\lambda_2 = k_{31} V^{-m}$ ($m = 0.33$–0.41)	
Zn–8 wt.% Al	2.8–12	53	0.15–0.64	$\lambda_1 = k_{32} G^{-0.57}$	
	2.8–12	100	0.28–1.2	$\lambda_1 = k_{33} G^{-0.052}$	
Ni base superalloy (IN738LC) [a]	5–8.5	16–333	0.08–2.8	$\lambda_1 = k_{34} (GV)^{-0.31}$	[12]
				$\lambda_2 = k_{35} (GV)^{-0.56}$	
Fe–(1.48C–1.14 Mn) wt.%	5.3	8–210	0.042–1.11	$\lambda_1 = k_{37} V^{-0.22}$	[57]
				$\lambda_2 = k_{38} G^{-0.48}$	
				$\lambda_2 = k_{39} V^{-0.45}$	
Fe–(0.59C–1.10 Mn) wt.%	5.5		0.044–1.15	$\lambda_1 = k_{40} V^{-0.29}$	
				$\lambda_1 = k_{41} G^{-0.72}$	
				$\lambda_2 = k_{42} G^{-0.51}$	
				$\lambda_2 = k_{43} G^{-0.45}$	
				$\lambda_2 = k_{44} V^{-0.45}$	
Zn–(1.54–2.79) wt.% Mg	15–95	10–21800	0.15–2071	$\lambda_2 = k_{45} V^{-0.33}$	[75]
Zn–(0.54–3.06) wt.% Mg	15	1–8000	0.015–120	$\lambda_2 = k_{46} V^{-0.33}$	[76]
SCN–2.5 wt.% ETH[b]	7.8	3–50	0.023–0.39	$\lambda_1 = k_{47} V^{-0.33}$	[13]
SCN–5.5 mol ACE[b]	6.7	0.4–100	0.003–0.67	$\lambda_2 = k_{48} V^{-0.56}$	[43]
SCN–1.3 wt.% ACE[b]	1.6–9.7	1.6–250	0.003–2.42	$R = k_{49} V^{-0.53}$	[63]

[a] Ni–(15.9 Cr–8.1 Co–3.3 Ti–3.4 Al–3W–1.9 Mo–1.6 Ta–0.8 Nb–0.11 C) wt.%.
[b] SCN, succinonitrile; ETH, ethanol; ACE, acetone.

predicted by Kurz–Fisher model [39], but the experimental results obtained in the Al–(6,24) wt.% Cu alloys were in poor agreement with the same models. The predicted R values of the Hunt model [38] and Trivedi model [40] are quite smaller than our experimental values. Similar results were also obtained by Kim et al. [37].

3.5. Mushy zone depth

The variation of d with G (at a constant $V = 9.5$ mm s^{-1}) and with V (at a constant $G = 6.3$ K mm^{-1}) for different Al–Cu alloys are shown in Fig. 14 and Table 1. It can be seen that the variation of d on the log d

versus log G and log d versus log V plots are linear. Fig. 14(a) shows that an increase in G produce decrease in d. A regression analysis gives the proportionality equation as $d = k_4 G^{-a4}$. The exponent value of a_4 equals to 0.47, 0.46, 0.60 and 0.58 for the Al–(3,6,15,24) wt.% Cu alloys, respectively ($\bar{a}_4 = 0.53 \pm 0.07$).

An increase in V also produce a decrease in d. As shown in Fig. 14(b) and Table 1, d varies with V in the same manner as λ_1 varies with V. Thus, we can describe the relationship between d and V by linear regression analysis as $d = k'_4 V^{-b4}$. The growth rate exponent value b_4 equals to 0.30, 0.35, 0.21 and 0.25 for the Al–(3,6,15,24) wt.% Cu alloys, respectively ($\bar{b}_4 = 0.28 \pm 0.05$). It appears that the exponent value of b_4 does not vary with C_o. The d values were found to be between 3.4–19 mm depending on G for Al–15 wt.% Cu alloy. The experimental d values changed between 1.4–29.4 mm depending on G, V and C_o values (Fig. 15 and Table 1). The experimental d values were smaller than d values (38 mm) obtained by Clyne [71] with Al–Cu alloys and were similar to d values (7.7–28 mm) obtained by Tewari et al. [70] with Pb–(27–34) wt.% Sn alloys. The results of the constitutional supercooling criterion [46,47] and the phase diagram data (calculated from Eq. (11)) are compared with the experimentally determined d, in Fig. 15. As can be seen from Fig. 15(a), the experimental results for the d values were in good agreement with the predicted results for the temperature gradient between 2.5–6.4 K mm^{-1}. The constitutional supercooling criterion and the phase diagram data predict monotonous change of d against G, though the experimental data shows a greater discrepancy when G gets smaller (Fig. 15(a)). The dependence of d on the initial alloy composition C_o for a constant $G = 6.3$ K mm^{-1} is given in Fig. 15(b). The experimental and the predicted d values increase with the increasing C_o until $C_o = 6$ wt.% Cu content and then decrease with the increasing C_o values. As can be seen from Fig. 15(b) a good agreement is obtained between the experimental d values and d values predicted from the phase diagram data for Al–6 wt.% Cu alloy and d values predicted from the constitutional supercooling criterion for Al–15 wt.% Cu alloy. In general, the experimental results show a similar trend with the predicted results.

4. Conclusion

Al–(3,6,15,24) wt.% Cu alloys were solidified unidirectionally upwards with a constant G (7.4 K mm^{-1}) at a wide range of V (9–490 μm s^{-1}) and with a constant V (9.5 μm s^{-1}) at a wide range of G (1.0–7.4 K mm^{-1}), and their microstructural features observed from the longitudinal and transverse views of the specimen studied for examining the influence of microstructural parameters (λ_1, λ_2, R, d) depend on solidification parameters (G, V, C_o). The principal results can be summarized as follows:

1. The primary dendrite arm spacing λ_1 decreases with increasing G for constant V and with increasing V for constant G in the Al–Cu alloys studied. A linear regression analysis gives the relationships as $\lambda_1 = k_1 G^{-a1}$ and $\lambda_1 = k'_1 V^{-b1}$. The gradient exponent $\bar{a}_1 = 0.43 \pm 0.10$ for our experimental results is significantly lower than the theoretical value (0.5); this aligns with the several experimental observations on other systems [9,10,12,54,55]. The growth rate exponent $\bar{b}_1 = 0.28 \pm 0.03$ is slightly higher than the theoretical value (0.25), this is also in accordance with the experimental observations on other systems [3–13,36,43,53–55].

2. The λ_1 values calculated by the Kurz–Fisher model [39] were too large compared to experimental results. The experimental λ_1 values were in good agreement with the calculated λ_1 values by the Trivedi model for lower Cu content (Al–(3,6) wt.% Cu) alloys whereas, the λ_1 values obtained by the Hunt model [38] agrees very well with the higher Cu content (Al–(15,24) wt.% Cu) alloys. The experimental results are in quite good agreement with the calculated λ_1 values by the Hunt–Lu model [33] especially for Al–(3,6,15) wt.% Cu alloys for the growth rates between 20–200 μm s^{-1}. However, the growth rates smaller than 20 μm s^{-1} and higher than 200 μm s^{-1} show significant discrepancies between the experimental and calculated λ_1 values.

3. This study shows that an increase in G at constant V and an increase in V at constant G for a given C_o produces a decrease in λ_2. A linear regression analysis gives the proportionality equations as $\lambda_2 = k_2 G^{-a2}$ and $\lambda_2 = k'_2 V^{-b2}$, a_2 was effected with the variation of C_o but b_2 ($\bar{b}_2 = 0.32 \pm 0.07$), and similar results were found in the literature (Table 2).

4. It was found that λ_2 and R decrease with the increasing $C_o V$. The variation of λ_2 and R with $C_o V$ at a constant G can be represented as $\lambda_2 = k(C_o V)^{-0.32}$ and $R = k'(C_o V)^{-0.43}$ and the value of λ_2/R for the $C_o V$ range studied in this work was 2.8 ± 0.4 which is in good agreement with the Huang and Glicksman result ($\lambda_2/R = 3.0$) [64] and significantly higher than the result (2.1) of Langer [94] and Müller-Krumbhaar and Langer [95].

5. The plots of log R versus log G at constant V and log R versus log V at constant G form a family of straight lines. Thus the mathematical relationships can be expressed as $R = k_3 G^{-a3}$ and $R = k'_3 V^{-b3}$. The exponent a_3 changes randomly with the variation of C_o whereas the exponent b_3 seems to decrease slightly with the increasing C_o. The relationships obtained between R and V in this work for Al–(3,6,15) wt.% Cu alloys is in good agreement with the relationships obtained by Miyata et al. [36] and Cattaneo et al. [42].

6. The experimental R values were in good agreement with the results obtained by the Kurz–Fisher

model [39] for the Al–(3,15) wt.% Cu alloys but were in poor agreement with the predicted values by the same model for the Al–(6,24) wt.% Cu alloys. The predicted R values with the Hunt model [38] and the Trivedi model [40] are quite smaller than our experimental values.

7. An increase in G at constant V and an increase in V at constant G produce a decrease in d for a given C_o. A regression analysis gives the proportionality equation as $d = k_4 G^{-a4}$ and $d = k'_4 V^{-b4}$. The exponent a_4 ($\bar{a}_4 = 0.53 \pm 0.07$) values seem to be effected slightly with C_o but the exponent b_4 ($\bar{b}_4 = 0.28 \pm 0.05$) values are not effected as much. The experimental d values changed between 1.4–29.4 mm (depending on G, V and C_o values) which were similar to the d values (7.7–28 mm) obtained by Tewari et al. [70] and were smaller than the d values (38 mm) obtained by Clyne [71].

8. The experimental d values were in good agreement with the predicted results from the constitutional supercooling criterion [46,47] for G between 3–6.4 K mm^{-1}. However, the constitutional supercooling criterion and the phase diagram values predict monotonous change of d against G, though the experimental data show a greater discrepancy when G gets smaller. The experimental and the predicted d value reaches its maximum at about $C_o = 6$ wt.% Cu content and then decreases with decreasing and increasing C_o values (Fig. 15(b)). When $C_o = 0$ and $C_o = C_E$, d value goes to zero because at these composition ΔT_o goes to zero, as expected from the phase diagram (Fig. 1) and Eq. (11).

Experimental studies carried out in different systems either metallic or organic, (Table 2), showed a slight variation of the temperature gradients exponent a_i and the growth rates exponent b_i from the theoretical calculations as also observed in our study. This might be due to the experimental producers, as well as the dependence of a_i and b_i on the particular alloy system and the alloy composition used.

Appendix A. Statistical results of the variation of microstructural parameters (λ_1, λ_2, R, d) with the solidification parameters (G, V)[a]

Relationships	Constants	Correlation coefficients
Composition: Al–3 wt.% Cu		
$\lambda_1^* = k_{1*} G^{-0.35}$	$k_{1*} = 6.0 \times 10^1$ ($\mu m^{0.65}$ °C $^{0.35}$)	$r_{1*} = -0.983$
$\lambda_1^* = k_{2*} V^{-0.32}$	$k_{2*} = 8.1 \times 10^2$ ($\mu m^{1.32}$ $s^{-0.32}$)	$r_{2*} = -0.992$
$\lambda_1^{**} = k_{3*} G^{-0.46}$	$k_{3*} = 3.1 \times 10^1$ ($\mu m^{0.54}$ °$C^{0.46}$)	$r_{3*} = -0.981$
$\lambda_1^{**} = k_{4*} V^{-0.31}$	$k_{4*} = 7.9 \times 10^2$ ($\mu m^{1.31}$ $s^{-0.31}$)	$r_{4*} = -0.992$
$\lambda_1 = k_1 G^{-0.41}$	$k_1 = 4.5 \times 10^1$ ($\mu m^{0.59}$ °$C^{0.41}$)	$r_1 = -0.983$
$\lambda_1 = k_2 V^{-0.32}$	$k_2 = 8.1 \times 10^2$ ($\mu m^{1.32}$ $s^{-0.32}$)	$r_2 = -0.993$
$\lambda_2 = k_3 G^{-0.39}$	$k_3 = 0.6 \times 10^1$ ($\mu m^{0.61}$ °$C^{0.39}$)	$r_3 = -0.920$
$\lambda_2 = k_4 V^{-0.46}$	$k_4 = 12.0 \times 10^1$ ($\mu m^{1.46}$ $s^{-0.46}$)	$r_4 = -0.984$
$R = k_5 G^{-0.51}$	$k_5 = 0.2 \times 10^1$ ($\mu m^{0.49}$ °C $^{0.51}$)	$r_5 = -0.984$
$R = k_6 V^{-0.60}$	$k_6 = 1.2 \times 10^2$ ($\mu m^{1.60}$ $s^{-0.60}$)	$r_6 = -0.982$
$d = k_7 G^{-0.47}$	$k_7 = 6.9 \times 10^2$ ($\mu m^{0.53}$ °C $^{0.47}$)	$r_7 = -0.974$
$d = k_8 V^{-0.30}$	$k_8 = 16.3 \times 10^3$ ($\mu m^{1.30}$ $s^{-0.30}$)	$r_8 = -0.952$
Composition: Al–6 wt.% Cu		
$\lambda_1^* = k_{5*} G^{-0.59}$	$k_{5*} = 1.9 \times 10^1$ ($\mu m^{0.41}$ °$C^{0.59}$)	$r_{5*} = -0.997$
$\lambda_1^* = k_{6*} V^{-0.26}$	$k_{6*} = 6.8 \times 10^2$ ($\mu m^{1.26}$ $s^{-0.26}$)	$r_{6*} = -0.994$
$\lambda_1^{**} = k_{7*} G^{-0.56}$	$k_{7*} = 2.2 \times 10^1$ ($\mu m^{0.44}$ °$C^{0.56}$)	$r_{7*} = -0.998$
$\lambda_1^{**} = k_{8*} V^{-0.29}$	$k_{8*} = 7.4 \times 10^2$ ($\mu m^{1.29}$ $s^{-0.29}$)	$r_{8*} = -0.997$
$\lambda_1 = k_9 G^{-0.57}$	$k_9 = 2.0 \times 10^1$ ($\mu m^{0.43}$ °$C^{0.57}$)	$r_9 = -0.999$
$\lambda_1 = k_{10} V^{-0.28}$	$k_{10} = 7.2 \times 10^2$ ($\mu m^{1.28}$ $s^{-0.28}$)	$r_{10} = -0.996$
$\lambda_2 = k_{11} G^{-0.62}$	$k_{11} = 0.15 \times 10^1$ ($\mu m^{0.38}$ °C $^{0.62}$)	$r_{11} = -0.987$
$\lambda_2 = k_{12} V^{-0.32}$	$k_{12} = 7.5 \times 10^1$ ($\mu m^{1.32}$ $s^{-0.32}$)	$r_{12} = -0.995$
$R = k_{13} G^{-0.74}$	$k_{13} = 8.3 \times 10^{-1}$ ($\mu m^{0.26}$ °C $^{0.74}$)	$r_{13} = -0.962$
$R = k_{14} V^{-0.56}$	$k_{14} = 1.1 \times 10^2$ ($\mu m^{1.56}$ $s^{-0.56}$)	$r_{14} = -0.993$
$d = k_{15} G^{-0.46}$	$k_{15} = 16.3 \times 10^2$ ($\mu m^{0.54}$ °$C^{0.46}$)	$r_{15} = -0.966$
$d = k_{16} V^{-0.35}$	$k_{16} = 38.8 \times 10^3$ ($\mu m^{1.35}$ $s^{-0.35}$)	$r_{16} = -0.967$

Appendix A. *(Continued)*

Relationships	Constants	Correlation coefficients
Composition: Al–15 wt.% Cu		
$\lambda_1^* = k_{9*}G^{-0.46}$	$k_{9*} = 3.1 \times 10^1$ ($\mu m^{0.54}$ $°C^{0.46}$)	$r_{9*} = -0.983$
$\lambda_1^* = k_{10*}V^{-0.23}$	$k_{10*} = 5.64 \times 10^2$ ($\mu m^{1.23}$ $s^{-0.23}$)	$r_{10*} = -0.979$
$\lambda_1^{**} = k_{11*}G^{-0.41}$	$k_{11*} = 4.2 \times 10^1$ ($\mu m^{0.59}$ $°C^{0.41}$)	$r_{11*} = -0.987$
$\lambda_1^{**} = k_{12*}V^{-0.23}$	$k_{12*} = 5.75 \times 10^2$ ($\mu m^{1.23}$ $s^{-0.23}$)	$r_{12*} = -0.986$
$\lambda_1 = k_{17}G^{-0.43}$	$k_{17} = 3.7 \times 10^1$ ($\mu m^{0.57}$ $°C^{0.43}$)	$r_{17} = -0.992$
$\lambda_1 = k_{18}V^{-0.23}$	$k_{18} = 5.75 \times 10^2$ ($\mu m^{1.23}$ $s^{-0.23}$)	$r_{18} = -0.982$
$\lambda_2 = k_{19}G^{-0.48}$	$k_{19} = 0.3 \times 10^1$ ($\mu m^{0.52}$ $°C^{0.48}$)	$r_{19} = -0.961$
$\lambda_2 = k_{20}V^{-0.39}$	$k_{20} = 8.1 \times 10^1$ ($\mu m^{1.39}$ $s^{-0.39}$)	$r_{20} = -0.990$
$R = k_{21}G^{-0.67}$	$k_{21} = 4.5 \times 10^{-1}$ ($\mu m^{0.33}$ $°C^{0.67}$)	$r_{21} = -0.991$
$R = k_{22}V^{-0.43}$	$k_{22} = 3.2 \times 10^1$ ($\mu m^{1.43}$ $s^{-0.43}$)	$r_{22} = -0.987$
$d = k_{23}G^{-0.60}$	$k_{23} = 4.0 \times 10^2$ ($\mu m^{0.40}$ $°C^{0.60}$)	$r_{23} = -0.983$
$d = k_{24}V^{-0.21}$	$k_{24} = 12.9 \times 10^3$ ($\mu m^{1.21}$ $s^{-0.21}$)	$r_{24} = -0.977$
Composition: Al–24 wt.% Cu		
$\lambda_1^* = k_{13*}G^{-0.31}$	$k_{13*} = 8.1 \times 10^1$ ($\mu m^{0.69}$ $°C^{0.31}$)	$r_{13*} = -0.935$
$\lambda_1^* = k_{14*}V^{-0.25}$	$k_{14*} = 6.58 \times 10^2$ ($\mu m^{1.25}$ $s^{-0.25}$)	$r_{14*} = -0.984$
$\lambda_1^{**} = k_{15*}G^{-0.30}$	$k_{15*} = 8.9 \times 10^1$ ($\mu m^{0.70}$ $°C^{0.30}$)	$r_{15*} = -0.989$
$\lambda_1^{**} = k_{16*}V^{-0.29}$	$k_{16*} = 7.81 \times 10^2$ ($\mu m^{1.29}$ $s^{-0.29}$)	$r_{16*} = -0.989$
$\lambda_1 = k_{25}G^{-0.30}$	$k_{25} = 8.8 \times 10^1$ ($\mu m^{0.70}$ $°C^{0.30}$)	$r_{25} = -0.971$
$\lambda_1 = k_{26}V^{-0.29}$	$k_{26} = 7.34 \times 10^2$ ($\mu m^{1.28}$ $s^{-0.28}$)	$r_{26} = -0.986$
$\lambda_2 = k_{27}G^{-0.70}$	$k_{27} = 6.4 \times 10^{-1}$ ($\mu m^{0.30}$ $°C^{0.70}$)	$r_{27} = -0.993$
$\lambda_2 = k_{28}V^{-0.27}$	$k_{28} = 3.6.10^1$ ($\mu m^{1.29}$ $s^{-0.29}$)	$r_{28} = -0.997$
$R = k_{29}G^{-0.70}$	$k_{29} = 4.4 \times 10^{-1}$ ($\mu m^{0.30}$ $°C^{0.70}$)	$r_{29} = -0.973$
$R = k_{30}V^{-0.39}$	$k_{30} = 2.9 \times 10^1$ ($\mu m^{1.39}$ $s^{-0.39}$)	$r_{30} = -0.997$
$d = k_{31}G^{-0.58}$	$k_{31} = 2.68 \times 10^2 \times$ ($\mu m^{0.42}$ $°C^{0.58}$)	$r_{31} = -0.936$
$d = k_{32}V^{-0.25}$	$k_{32} = 6.60 \times 10^3 \times$ ($\mu m^{1.25}$ $s^{-0.25}$)	$r_{32} = -0.997$
The variation of λ_2 and R with C_oV at constant G (6.3 K mm^{-1})		
$\lambda_2 = k_{33}(C_oV)^{-0.32}$ ($V = 19$ μm s^{-1} = Const.)	$k_{33} = 1.25 \times 10^2$ ($\mu m^{1.32}$ wt.%$^{0.32}$ $s^{-0.32}$)	$r_{33} = -0.872$
$\lambda_2 = k_{34}(C_oV)^{-0.39}$ ($C_o = 6$ wt.% Cu = Const.)	$k_{34} = 2.32 \times 10^2$ ($\mu m^{1.39}$ wt.%$^{0.39}$ $s^{-0.39}$)	$r_{34} = -0.990$
$R = k_{35}(C_oV)^{-0.40}$ ($V = 45$ μm s^{-1} = Const.)	$k_{35} = 1.62 \times 10^2$ ($\mu m^{1.40}$ wt.%$^{0.40}$ $s^{-0.40}$)	$r_{35} = -0.963$
$R = k_{36}(C_oV)^{-0.43}$ ($C_o = 15$ wt.% Cu = Const.)	$k_{36} = 1.01 \times 10^2$ (μm $^{1.43}$wt.%$^{0.43}$ $s^{-0.43}$)	$r_{36} = -0.987$

[a] λ_1^*, obtained with the Triangle Method; λ_1^{**}, obtained with the Area Counting Method; λ_1, obtained from average values of the area counting method and the triangle method.

Appendix B. Values of the physical parameters used in the calculation

$D = 3 \times 10^3$	(μm^2 s^{-1})		[39]
$k = 0.14$			[39]
$\Gamma = 0.241$	(K μm)		[84]
$m_\alpha = -2.72$	(K/wt.%)	for Al–3wt.%Cu	[a]
$m_\alpha = -2.74$	(K/wt.%)	for Al–6wt.%Cu	[a]
$m_\alpha = -2.76$	(K/wt.%)	for Al–15wt.%Cu	[a]
$m_\alpha = -3.57$	(K/wt.%)	for Al–24wt.%Cu	[a]

[a] Calculated from the phase diagram [78].

References

[1] F. Yılmazd, R. Elliott, J. Mater. Sci. 24 (1989) 2065.
[2] R.N. Grugel, Metall. Trans. 26A (1995) 496.
[3] A. Geying, L. Lixin, J. Cryst. Growth 80 (1987) 383.
[4] R.M. Sharp, A. Hellawell, J. Cryst. Growth 11 (1971) 77.
[5] D.G. McCartney, J.D. Hunt, Acta Metall. 29 (1981) 1851.
[6] M.D. Dupouy, D. Camel, J.J. Favier, Acta Metall. 40 (1992) 1791.
[7] X. Lin, W. Huang, J. Feng, T. Li, Y. Zhou, Acta Metall. 47 (1999) 3271.
[8] J.T. Mason, J.D. Verhoeven, R. Trivedi, J. Cryst. Growth 59 (1982) 516.
[9] C.M. Klaren, J.D. Verhoeven, R. Trivedi, Metall. Trans. 11A (1980) 1853.

[10] Y.L. Liu, S.B. Kang, Mater.Sci. and Tech. 13 (1997) 331.
[11] D. Liang, W. Jie, H. Jones, J. Cryst. Growth 135 (1994) 561.
[12] A. Kermanpur, N. Varahraam, E. Engilehei, M. Mohammadzadeh, P. Davami, Mater. Sci. Tech. 16 (2000) 579.
[13] W. Huang, X. Geying, Y. Zhou, J. Cryst. Growth 134 (1993) 105.
[14] Y.S. Han, D.H. Kim, H.I. Lee, Y.G. Kim, Scripta Metall. 31 (1994) 1623.
[15] N.F. Dean, A. Mortensen, M.C. Flemings, Metall. Trans. 25A (1994) 2295.
[16] J.A. Horwath, L.F. Mondolfo, Acta Metall. 10 (1962) 1037.
[17] S. DeCheveigne, C. Guthmann, M.M. Lebrun, J. Cryst. Growth. 73 (1985) 242.
[18] S. DeCheveigne, C. Guthmann, P. Kurowski, E. Vicente, H. Biloni, J. Cryst. Growth 92 (1988) 616.
[19] W.A. Tiller, J.W. Rutter, Can. J. Physics 34 (1956) 96.
[20] G.L. Ding, W.D. Huang, X. Huang, X. Lin, Y.H. Zhou, Acta Metall. 44 (1996) 3705.
[21] S.A. Moir, H. Jones, Mater. Lett. 12 (1991) 142.
[22] C.T. Rios, R. Caram, J. Cryst. Growth 174 (1997) 65.
[23] L.X. Liu, J.S. Kirkaldy, J. Cryst. Growth 140 (1994) 115.
[24] M.A. Eshelman, V. Seetharaman, R. Trivedi, Acta Metall. 36 (1988) 1165.
[25] X. Wan, Q. Han, J.D. Hunt, Acta Metall. 45 (1997) 3975.
[26] M. Vijayakumar, S.N. Tewari, J.E. Lee, P.A. Curreri, Mater. Sci. Eng. A132 (1991) 195.
[27] W.W. Mullins, R.F. Sekerka, J. App. Physics. 35 (1964) 444.
[28] M.H. Burden, J.D. Hunt, J. Cryst. Growth 22 (1974) 99.
[29] J.D. Hunt, Acta Metall. 38 (1990) 411.
[30] J.D. Hunt, Acta Metall. 39 (1991) 2117.
[31] S.-Z. Lu, J.D. Hunt, J. Cryst. Growth 123 (1992) 17.
[32] J.D. Hunt, S.-Z. Lu, Mater. Sci. Eng. A173 (1993) 79.
[33] J.D. Hunt, S.-Z. Lu, Mater. Sci. Eng. Metall. Trans. 27A (1996) 611.
[34] L. Yu, G.L. Ding, J. Reye, S.N. Ojha, S.N. Tewari, Metall. Trans. 31A (2000) 2275.
[35] S.N. Tewari, R. Shah, Metall. Trans. 27A (1996) 1353.
[36] Y. Miyata, T. Suzuki, J.I. Uno, Metall. Trans. 16A (1985) 1799.
[37] H.K. Kim, J.C. Earthman, E.J. Lavernia, Mater. Sci. Eng. A152 (1992) 240.
[38] J.D. Hunt, Solidification and Casting of Metals, The Metal Society, London, 1979, p. 3.
[39] W. Kurz, D.J. Fisher, Acta Metall. 29 (1981) 11.
[40] R. Trivedi, Metall. Trans. 15A (1984) 977.
[41] R. Trivedi, K. Somboonsuk, Mater. Sci. Eng. 65 (1984) 65.
[42] C.A. Cattaneo, O.P. Evequoz, H.R. Bertorello, Scripta Metall. 31 (1994) 461.
[43] K. Somboonsuk, J.T. Mason, R. Trivedi, Metall. Trans. 15A (1984) 967.
[44] R. Trivedi, W. Kurz, Acta Metall. 42 (1994) 15.
[45] V. Seetharaman, L.M. Fabietti, R. Trivedi, Metall. Trans. 20A (1989) 2567.
[46] J.W. Rutter, B. Chalmers, Can. J. Physics 31 (1953) 15.
[47] W.A. Tiller, K.A. Jackson, J.W. Rutter, B. Chalmers, Acta Metall. 1 (1953) 428.
[48] M.H. Burden, J.D. Hunt, J. Cryst. Growth 22 (1974) 109.
[49] E. Çadırlı, N. Marasli, B. Bayender, H. Sisman, M. Gündüz, J. Mater. Sci. 34 (1999) 5533.
[50] E. Çadırlı, N. Marasli, B. Bayender, M. Gündüz, Mater. Res. Bull. 35 (2000) 985.
[51] J.A. Warren, J.S. Langer, Phys. Review A. 42 (1990) 3518.
[52] K.P. Young, D.H. Kirkwood, Metall. Trans. 6A (1975) 197.
[53] M.A. Taha, Metal Sci. 13 (1979) 9.
[54] R.J. Su, R.A. Overfelt, W.A. Jemian, Metall. Trans. 29A (1998) 2375.
[55] E. Çadırlı, M. Gündüz, J. Mater. Sci. 35 (2000) 3837.
[56] H. Tunca, R.W. Smith, J. Mater. Sci. 23 (1988) 111.
[57] H. Jacobi, K. Schwerdtfeger, Metall. Trans. 7A (1976) 811.
[58] D. Bouchard, J.S. Kirkaldy, Metall. Trans. 28B (1997) 651.
[59] T. Okamoto, K. Kishitake, J. Cryst. Growth 29 (1975) 137.
[60] S. Ozbayraktar, A. Koursaris, Metall. Trans. 27B (1996) 287.
[61] H.S. Whitesell, L. Li, R.A. Overfelt, Metall. Trans. 31B (2000) 547.
[62] J.S. Langer, H. Müller-Krumbhaar, Acta Metall. 26 (1978) 1681.
[63] H. Esaka, W. Kurz, J. Cryst. Growth 71 (1985) 578.
[64] S.C. Huang, M.E. Glicksman, Acta Metall. 29 (1981) 701.
[65] H. Honjo, Y. Sawada, J. Cryst. Growth 58 (1982) 297.
[66] R.M. Sharp, A. Hellawell, J. Cryst. Growth 6 (1970) 253.
[67] S.N. Tewari, Mater. Sci. Eng. A130 (1990) 219.
[68] V. Laxmanan, Acta Metall. 33 (1985) 1023.
[69] V. Laxmanan, Acta Metall. 33 (1985) 1037.
[70] S.N. Tewari, R. Shah, H. Song, Metall. Trans. 25A (1994) 1535.
[71] T.W. Clyne, Mater. Sci. Eng. 65 (1984) 111.
[72] C.J. Paradies, R.N. Smith, M.E. Glicksman, Metall. Trans. 28A (1997) 875.
[73] I. Farup, A. Mo, Metall. Trans. 31A (2000) 1461.
[74] B. Goyeau, T. Benihaddadene, D. Gobin, M. Quintard, Metall. Trans. 30B (1999) 613.
[75] H.Y. Liu, H. Jones, J. Mater. Sci. Lett. 11 (1992) 769.
[76] H.Y. Liu, H. Jones, Acta Metall. 40 (1992) 229.
[77] T.F. Bower, H.D. Brody, M.C. Flemings, Trans. AIME. 236 (1966) 624.
[78] T. Lyman, Metals Handbook, American Society for Metals, Metals Park, OH, 1973.
[79] W. Kurz, D.J. Fisher, Fundamentals of Solidification, Trans Tech Publications, Aedermannsdorf, Switzerland, 1989, p. 16.
[80] McCartney D.G. Ph.D.Thesis, Oxford University, 1981 86.
[81] E. Çadırlı, A. Ülgen, M. Gündüz, Materials Transactions, JIM 40 (1999) 989.
[82] S. Ganesan, C.L. Chan, D.R. Poirier, Mater. Sci. Eng. A151 (1992) 97.
[83] M.S. Bhat, D.R. Poirier, J.C. Heinrich, Metall. Trans. 26B (1995) 1049.
[84] M. Gündüz, J.D. Hunt, Acta Metall. 33 (1985) 1651.
[85] J.J.G. Hsia, G.C.Y. Wang, in: Y.S. Touloukian (Ed.), Nonferrous Alloys, vol. 2, Macmillan, New York, 1970, p. 910.
[86] D.R. Poirier, S. Ganesan, Mater. Sci. Eng. A157 (1992) 113.
[87] M.H. Burden, J.D. Hunt, Metals Sci. 10 (1976) 156.
[88] H. Nguyen Thi, B. Billia, L. Capella, J. Physique 51 (1990) 625.
[89] McCartney D.G. PhD thesis, Oxford University, 1981 117.
[90] M.H. Burden, D.J. Hebditch, J.D. Hunt, J. Cryst. Growth 20 (1973) 121.
[91] S.N. Tewari, M.A. Chopra, J. Cryst. Growth 118 (1992) 183.
[92] P. Magnin, R. Trivedi, Acta Metall. 39 (1991) 453.
[93] G.R. Kottler, K.W. Casey, G.S. Cole, Metall. Trans. 3 (1972) 723.
[94] J.S. Langer, Rev. Mod. Phys. 52 (1980) 1.
[95] J.S. Langer, H. Müller-Krumbhaar, Acta Metall. 26 (1978) 1697.
[96] M.E. Glicksman, N.B. Singh, ASTM STP 890, ASTM, Philadelphia, PA, 1986, p. 44.
[97] T.Z. Kattamis, J. Coughlin, M.C. Flemings, Trans. Met. Soc. AIME. 239 (1967) 1504.
[98] M. Kahlweit, Scripta Metall. 2 (1968) 251.
[99] A. Mortensen, J.A. Cornie, M.C. Flemings, Metall. Trans. 19A (1988) 709.
[100] A. Mortensen, Metall. Trans. 22A (1991) 569.
[101] M. Chen, T.Z. Kattamis, Mater. Sci. Eng. A247 (1998) 239.
[102] V.R. Voller, J. Cryst. Growth 197 (1999) 333.